BRITISH GEOLOGICAL SURVEY

Engineering Geology and Geophysics Series

TECHNICAL REPORT WN/93/30

TWO-DIMENSIONAL INVERSION OF VLF-EM DATA

David Beamish

Author:
D. Beamish
BGS, Keyworth

This report was funded, in part, by the Commission of the European Communities.

Bibliographic Reference :
Beamish, D., 1993. Two-dimensional inversion of VLF-EM data.

British Geological Survey Technical Report WN/93/30.

British Geological Survey, Keyworth, Nottingham, 1993

Summary

This report was prepared as part of research programme funded in part by the Commission of the European Communities, European Coal and Steel Contract (EC Contract No. 7220 - AF/136). A number of geophysical methods have been applied to a sequence of test areas in the vicinity of Saarbrucken, Germany. The studies relate to methods for the recognition of geological weakness zones and other surface discontinuities caused by underground mining in Carboniferous terrain. Progress to date (October, 1993) is summarised by Greenwood and Peart (1992).

This report discusses a new method of data modelling applied to VLF data collected along three short (50 m) profiles in Saar Test Area 2.1. The data used in the study have previously been described by Greenwood and Peart (1992). The main aim of the report is to demonstrate an automatic method for the construction of a resistivity cross-section when suitable VLF-R data are supplied.

The method used (two-dimensional, non-linear, regularised inversion) has not been used previously in an applied geophysical context. This report therefore discusses the scientific rationale and the known pitfalls of the procedure. The method is also applied to both synthetic models and the field data in order to assist in the interpretation of the results obtained.

Introduction

The VLF survey technique is a well-established electromagnetic (EM) method of applied geophysics. Its use for geological and hydrogeological applications is reviewed by McNeill (1990). The method is one of a class of EM techniques that conform to a plane-wave sounding of subsurface resistivity structure; a closely allied (natural-field) technique is the audiomagnetotelluric (AMT) method (e.g. Strangway et al., 1973). The VLF-EM technique makes use of one or more distant radio transmitters operating between 15 and 30 kHz. The limited bandwidth means that, although several measurements may be obtained at different frequencies (using different transmitters), a main attribute of the method is that of a single frequency sounding. The lack of bandwidth is compensated for by the fact that the instrumentation is very portable and cost-effective. An extensive surveying capability is provided by a single, roving operator.

The VLF method was developed as an inductive sounding technique measuring the amplitude and (subsequently) phase relationship between the vertical (secondary) magnetic field (Z) relative to the horizontal primary field (H). This method, referred to here as VLF-Z, relies on wavefield interaction with two-dimensional (2-D) and three-dimensional (3-D) resistivity structure. The technique has since been extended to include a measure of the induced horizontal electric field (E) component. This VLF-R measurement provides an impedance value (e.g. E/H), usually expressed as apparent resistivity and phase, using short (e.g. 5 m) electric dipoles. The VLF-R measurement, although appropriate for a one-dimensional (1-D) application, contains only marginal information on the vertical resistivity structure (Fischer et al., 1983) because, in effect, only a single frequency is available. These factors suggest that the strength of VLF methods lie predominantly in the definition of lateral gradients in the subsurface resistivity structure. The interpretation problem is therefore, at least, two-dimensional.

Although extensive and high-density VLF data sets have been used successfully for *mapping* purposes (e.g. Ogilvy et al., 1991; Tabbagh et al., 1991), techniques which assess the third (i.e. depth) dimension appear both limited and restrictive. Here, as advocated by Fischer et al. (1983), a 2-D modelling (in this case inversion) approach to VLF interpretation is demonstrated using synthetic and field examples. The main aim is to demonstrate an automatic method for the construction of a resistivity cross-section using VLF-R data.

The general problem of EM induction, either by highly-polarised (VLF) or natural-source plane-wave fields requires vector measurements to fully specify the problem. The VLF technique has a directional limitation in that the horizontal magnetic field is conventionally measured in a direction perpendicular to the line of the transmitter and the associated E-field is measured along the line of the transmitter (essentially to ensure maximum signal strength). These limitations and the difficulties of interpretation that ensue have been extensively discussed by Tabbagh et al. (1991).

The close association between the VLF technique and the wide-band, natural-source magnetotelluric (MT) and AMT technique has been noted on many occasions. From the perspective of the MT technique the VLF method presents us with a directional set of VLF-R and/or VLF-Z measurements at a single frequency. Profile data is assumed. The objective is then to determine a resistivity cross-section that fits the measured data. When developing an inverse modelling approach, the recurring pitfalls of inaccurate, insufficient and inconsistent data (Jackson, 1972) must be appreciated. In a 2-D inverse problem which attempts to construct a valid depth cross-section, the use of single frequency data guarantees some level of insufficiency (the actual level will be case-specific). Care must also be exercised since the VLF data are directional and the data may be inconsistent with the modes presented by a 2-D problem as outlined below.

As discussed by Fischer et al. (1983), in order to ensure consistency with a 2-D approach, the directional VLF data must conform to one of the two principal modes of 2-D induction. The assumption of infinite strike (which defines the 2-D case) provides two decoupled modes involving separate combinations of the field components. The TE-mode (or E-polarisation, electric field parallel to strike) involves surface fields of Ex, Hy and Hz. The TM-mode (or H-polarisation, magnetic field parallel to strike) involves the surface fields Hx, Ey and Ez. Due to the directional nature of VLF measurements, we require therefore that the measurements be made in, at least one, of the two principal directions. Where the geological strike is not known, the sensible survey option of taking measurements from several azimuthally-distinct transmitters is suggested.

The present study comprises an initial discussion on the developments which have taken place in MT data modelling using regularised inversion techniques. Such procedures provide (in fact impose) smooth models of the subsurface resistivity distribution. These smooth models are intended to provide lower bounds on the amount of structure required to fit the data and, as such, tend to reduce the problem of equivalence that is a component part of employing diffusive EM wavefields. Smooth, minimum-structure resistivity cross-sections are not yet a familiar concept in applied geophysics. In order to provide insight into their practical application to VLF data, both synthetic and field data examples are considered.

Regularised Inversion

The starting point in the modelling of VLF data are the developments in non-linear inversion which have arisen in the context of the multi-frequency MT technique. The new approaches, developed first for the 1-D MT problem and more recently for 2-D geometries, involve regularising an otherwise 'ill-posed' problem by introducing a smooth or minimum-structure constraint. In these methods the subsurface resistivity structure is constrained to vary smoothly and we seek the resistivity distribution with the minimum amount of structure (roughness) that fits the observations. The approach is effective because measured data are invariably limited in number and precision (insufficient and inaccurate) and because the EM

wavefield is diffusive. These two factors ensure that pointwise discontinuities (e.g. layers/polygons) in the subsurface cannot be resolved without a degree of equivalence. In 2-D modelling and inversion, the problem of equivalence becomes particularly acute because of the larger number of degrees of freedom within the model space. The essential point is that the minimum-structure inversion concept acknowledges this fact and allows the automatic construction of credible (non-extreme) resistivity models.

In the 1-D case, formulations of the inverse MT problem when the vertical resistivity profile is rigorously smooth (e.g. in terms of its first and second derivatives) have been considered by Constable et al. (1987) and by Smith and Booker (1988). For 2-D MT inversion, deGroot-Hedlin and Constable (1990) implemented a minimum-structure inversion which is referred to as OCCAM and is based on the finite-element forward solution of Wannamaker et al. (1987). A more rapid 2-D MT inversion called the Rapid Relaxation Inverse has also been developed by Smith and Booker (1991). Here we use the 2-D OCCAM procedure, described in detail by deGroot-Hedlin and Constable (1990), which has proved to be a very stable algorithm.

It is important that the measured data should possess associated error bounds. The underlying concept is that we should *never* attempt to obtain an *exact* fit between measured and modelled data. The error bound must comprise the variance associated with physical measurement but it can also encompass the degree to which a particular level of modelling (e.g. 1-D, 2-D or 3-D) is thought to be appropriate. Given a set of N observations (o_i, i=1,N) with standard errors (σ_i) , the concept is to only fit the observations to within a prescribed level of misfit. When the data and errors conform to Gaussian behaviour the chi-square (χ^2) statistic is a natural measure of misfit :

$$\chi^2 = \sum | o_i - m_i |^2 / \sigma_i^2$$

where m_i refers to the i'th model response. For a model fit to be satisfactory we might typically take $\chi^2 < N + 2(2N)^{1/2}$ (Parker and Whaler, 1981). This would correspond to accepting models whose misfit is less than two standard errors of χ^2 above its expected value of N. Here we use an r.m.s. measure of misfit defined as χ^2/N with an expectation value of unity.

Smooth, minimum-structure resistivity cross-sections are not yet a familiar concept in applied geophysics. In order to provide some insight into their practical application to VLF data both synthetic and field data are considered. As noted previously, single-frequency profile data present a special case of data insufficiency and it is important to first diagnose the resolution attributes of this special case using synthetic examples.

For consistency, both synthetic examples and field data have been treated using an equivalent formulation of the problem. The field data consist of only 11 observations (along 3 parallel

profiles) at 5 m separations across a 50 m baseline. The synthetic data, obtained by the forward-modelling scheme of Wannamaker et al. (1987), have been generated at an equivalent set of 11 locations. In all cases, the parameterisation of the inversion model space is the same. The central portion of the model (50 m x 50 m) consists of a regularisation grid containing individual blocks of a width and thickness of 2.5 m. This parameterisation obviously sets a limit in terms of the minimum-scale of any resolvable features.

Both synthetic and field inversion results are presented in true scale across the 50 m x 50 m central section. Although the inversion grid comprises 2.5 m x 2.5 m rectangular blocks, results are block contoured at a interval of 1 m. In each case a uniform half-space is used to initiate the inversion i.e. we are considering the case of *automatic* inversion. Constraints which may provide increased resolution are available within the inversion algorithms but are not discussed here.

Synthetic Example 1.

This example is primarily intended to demonstrate the nature of minimum-structure cross-sections using one mode and one or two VLF frequencies. It can be assumed that two VLF frequencies can be used to provide only a limited frequency separation. Depending on the transmission azimuths, the data might provide results in two separate modes (i.e. both TE and TM and transmission paths orthogonal) or in the same single mode (transmission paths parallel). We here consider the case of observations made at two frequencies (16 and 25 Khz) which provide the same (TE) mode of induction.

The model (see Fig. 2) is a simple conductive zone buried in a half-space. The conductive zone has a resistivity of 5 ohm.m and is immersed in 100 ohm.m material. The upper surface of the anomaly is at 10 metres and it extends to 20 metres (i.e. a thickness of 10 m). The anomaly is, in effect, a laterally elongate zone (extending to infinity) and we examine the resolution of measurements made over the rectangular terminating edge of the concealed zone.

The anomaly has a resistivity contrast of 20 and skin-depths in the zone range from 8.89 m at 16 kHz to 7.11 at 25 kHz. The skin-depths at these frequencies are comparable to the thickness of the anomaly and a strong inductive response will be observed. In the background material skin-depths range from 39.76 m (16 kHz) to 31.81 m (25 kHz). Clearly the electrical scale-lengths are very similar for the two frequencies.

We consider 11 observations made at 5 m separations, over a total baseline of 50 m. The observational anomaly for the TE-mode at 16 and 25 kHz is shown for apparent resistivity and phase in Figure 1 (symbols). The edge of the anomaly is situated at -150 m in model coordinates (Fig. 2). Examination of Figure 1 demonstrates that a 50 m baseline is insufficient to fully define the spatial wavelength of the anomaly. With increasing distance

from the edge of the anomaly the response must revert to the corresponding half-space response (an apparent resistivity of 100 ohm.m and a phase of 45 degrees). For this model example the 11 synthetic observations, although accurate, are insufficient in terms of spatial scale.

A series of investigations into the resolution of the data were made using the 2-D OCCAM algorithm. Only the resolution of the TE-mode is reported here. In each case a 'blind' starting model consisting of a half-space of 30 ohm.m was used. Data errors (in the logarithm of apparent resistivity and in linear phase) were set at 1%.

The model cross-section obtained at an r.m.s. misfit of unity, using the TE-mode at 16 kHz only, is shown in Figure 2. The cross-section is in true scale and the logarithm of resistivity is contoured. The target conductive zone is outlined by the heavy dashed line. A blank (white) zone is used here to denote resistivity overshoot i.e. where model resistivities are less than the target resistivity of 5 ohm.m. The lightest gray-scale denotes model resistivities greater than the true background of 100 ohm.m.

The model returned by the inversion is necessarily smooth and consists of a series of gradients with associated spatial wavelengths. In very broad terms the minimum-structure solution can be seen to be 'generally' consistent with the starting model when given (i) accurate data (i.e. synthetic and no-noise data) and (ii) insufficient and inadequate data (i.e. only one mode, one frequency and a limited spatial wavelength).

The resolution obtained in this example can be summarised as follows. The first reflecting horizon (the upper surface of the conductive zone) is the best resolved feature. Since only one frequency is used to constrain the solution, subsequent vertical resolution (e.g. the lower surface of the conductive zone) is more limited. The most conductive feature of the solution is likely to be displaced downwards from the 'true' centre and inwards from the 'true' edge. The 'edge effect' consists of a set of gradients that are 'more realistic' in the upper portion of the section. The resolution through the lower part of the section is very limited.

It should be noted that a highly accurate solution can be obtained by the OCCAM inversion, particularly using synthetic data. This is achieved by providing multi-frequency profile data that 'best-suit' the electrical scale of the problem. For our present purposes we wish to consider typical resolution attributes of the limited type of data that would be supplied by routine VLF data sets.

A model cross-section obtained using the TE-mode data and the two VLF frequencies of 16 and 25 kHz is shown in Figure 3. The r.m.s. misfit of the solution is again unity. The introduction of the *higher* frequency (in the same mode) in this example has increased the resolution of the target, particularly through the upper part of the section but also generally throughout the section.

In this example near-surface resistivities of the correct half-space value (100 ohm.m) are returned by the inversion and the most conductive feature is centred on the target anomaly. The lowest individual (2.5 x 2.5 m) block resistivity in the conductive zone is 3.5 ohm.m which compares favourably with the actual value of 5 ohm.m.

The response of the model for both frequencies and an r.m.s. misfit of unity, is compared with the observed synthetic data set in Figure 1. It should be noted that the misfit is an 'overall' figure and is, inevitably, distributed over the 44 observations. It can be seen that there is scope for further matching between the observed and modelled data, particularly in the phase response at 25 kHz.

For this example it has proven possible to 'overfit' the synthetic data by a factor of two, producing a stable solution at an r.m.s. misfit of 0.5 with the same 1% errors assigned to the data. The resulting model, using the same data as in the previous case is shown in Figure 4. The increase in structural resolution over the previous case is only marginal.

Synthetic Example 2.

This example is primarily intended to demonstrate the nature of minimum-structure cross-sections using one or two of the different modes that may be observed at a single frequency. The anomaly studied is more complex than that of the previous case in that it consists of an isolated conductive zone dipping at about 45 degrees. The structure, which simulates a dipping fault zone, is a typical application for VLF observations. The model was developed as a control for the interpretation of the field data modelling discussed later.

The model (see Fig. 7) is again a simple conductive zone of 5 ohm.m immersed in a material of 100 ohm.m. The top of the zone is set at 2 m and has a width of approximately 5 m. The zone dips at an angle of about 45 degrees down to a depth of 20 m. The scale of the anomalous structure has dimensions (5 and 18 m) both less than and greater than one skin-depth of a 16 kHz wavefield within the anomalous zone (8.89 m).

We again consider 11 observations made at 5 m separations over a total baseline of 50 m which is centred above the anomalous region. The observational anomaly for the TE- and TM-modes at 16 kHz is shown in Figure 5. The vertical field (Z) response (real and imaginary components) produced in the TE-mode is shown Figure 6. It should be noted that in Figures 5 and 6 the solid lines are simply data traces (they are not inversion results). The asymmetry in all the response data, produced by the dipping anomaly, is very evident. For this type of anomaly, the spatial wavelengths of the anomalous response decrease as TM-mode < TE-mode < Z (TE-mode). For a sufficient coverage of the anomalous region we would require the apparent resistivities to return to 100 ohm.m, the phases to return to 45 degrees and the Z-field to return to zero.

As in the previous example, a series of investigations into the resolution of the data were made using the 2-D OCCAM algorithm. Again, a 'blind' starting model consisting of a half-space of 30 ohm.m was used throughout. Data errors of 1% were again assumed. Although 'more accurate' solutions have been obtained, the solutions obtained at an r.m.s. misfit of unity are presented. It will be noted that the contour level scheme is almost the same as that used in the previous example (model resistivities are the same). Here a lower bound of 0.75 (logarithmic scale) is used since, for this example, modelled resistivities approach, but do not achieve, the target resistivity of 5 ohm.m.

The model cross-section obtained at an r.m.s. misfit of unity using the TE-mode data (apparent resistivity and phase) at 16 Khz is shown in Figure 7. The cross-section is true scale and the logarithm of resistivity is contoured. The target conductive zone is outlined by the heavy dashed line. With only one frequency constraining the solution, the imaging of a dipping zone will inevitably be difficult. In broad terms, the smooth solution returns an asymmetrical conductive zone. The upper surface of the zone (first reflecting horizon) is well resolved and the upper surface of the dipping zone is imaged by a gradient whose dip is close to that of the target zone. Elsewhere, through the upper part of the section, the trace of the most conductive zone in the model is closer-to-vertical than the actual dip. As was the case in the previous model, the resolution through the lower part of the section is very limited.

The equivalent cross-sectional model obtained using the TM-mode data is shown in Figure 8. The model obtained has broadly similar characteristics to that obtained from the TE-mode data. In detail, the set of gradients in the vicinity of the low resistivity zone appear to 'contain' the true dip in a more satisfactory manner.

The modelling investigation of the TE-mode data can be extended by assuming that vertical field data are also available. This increases the number of observational constraints by a factor of 2 (from 22 to 44, for the 11 site profile). The cross-sectional model obtained using the TE-mode R and Z data at 16 kHz is shown in Figure 9. The increase in true structural resolution over that obtained using only the TE-mode R data is only marginal.

As in the previous example, we might also assume that two VLF frequencies can be recorded. In this final synthetic example we consider the case in which observations of two frequencies (15 and 30 kHz) have been obtained in the same TM-mode (i.e. the VLF transmissions had very similar azimuths). As in the previous example, it should be noted that two frequencies provide similar skin-depths in the two model regions.

The resulting model, obtained at a misfit of unity, is shown in Figure 10. The cross-section probably represents the 'most-realistic' image obtained, thus far, by the minimum-structure inversion. The image of an isolated dipping conductive zone in an otherwise uniform background is clearly well-represented by the gradients obtained. Once again the upper surface of the conductive zone (first wavefield contact with the anomaly) is the best-imaged feature. The 'more-resistive' zone to the right of the true anomaly is thought to be due to

Gibb's phenomenon (i.e. trying to fit a smooth model to a feature exhibiting sharp discontinuities can result in model overshoot).

In summary, for the dipping model studied, complete resolution of the 'true' structure is difficult when only one VLF frequency is involved. For the model studied both TE- and TM-mode data provide similar resolution attributes. As in the previous example, the first reflecting horizon is the best resolved feature. The upper surface of the dipping zone is then imaged by a gradient whose dip is close to that of the target zone. A series of 'false', near-vertical gradients project downwards from the upper surface. In all cases the minimum resolved resistivities occur *within* the anomalous zone, close to the upper surface. The values of the lowest resistivities appear to be marginally higher than the true resistivities.

Application to field data.

The data studied here were collected as part of a collaborative study into geophysical methods for the recognition of geological weakness zones and other surface discontinuities caused by underground mining in Carboniferous terrain (Greenwood and Peart, 1992). In one of the study areas (Saar 2.1, Test Site 3) three profiles of VLF-R and Z measurements were made.

The three profiles are shown in Figure 11 (plan-view) and were made along azimuths of N59E. The three profiles are 50 metres in length, are separated by 10 metres, and each comprise 11 measurements made at 5 metre intervals. The profiles are referred to as 00S, 10S and 20S. The lateral, along-profile, coordinates range from -175 to -125 m. Also shown in Figure 11 is a possible fault trace based on a 10 cm topographic feature.

The measurements were made with the Scintrex IGS-2 equipment, using 5 metre E-field dipoles and the Rugby (UK) VLF transmitter (GBR, 16 kHz). The transmission azimuth, along which E-field dipoles were aligned was 320 degrees. The equipment has a reading resolution of 1% in the case of the VLF-Z components and 1 ohm.m and 1 degree in the case of the VLF-R measurements.

The map of Figure 11 also displays the in-phase Z results that were obtained. Both in-phase and in-quadrature (not shown) Z fields are small and consistently less than 7% of the associated horizontal component. In addition, it can be noted from Figure 11, that there is no convincing (i.e. strong) sign reversal in the in-phase component. Such a characteristic is the normal signature when traversing a lateral discontinuity (e.g. Fig. 6).

The VLF-R data obtained along the 3 profiles are shown in Figures 12, 13 and 14. The observational results are indicated by symbols and the full and broken lines are model results which are discussed later. As explained previously it is necessary to assign errors to the data observed. The data shown in Figures 12 to 14 have had 'nominal' 2.5% error bounds applied

(in the logarithm of apparent resistivity and in linear phase).

Despite the separation of only 10 metres between successive profiles there are very clear differences in the behaviour of the response characteristics across the three sets of observations. A clear minimum in apparent resistivity is observed along profiles 00S and 10S but along 20S the form of response is a step. The phase response along profiles 00S and 10S shows a clear similarity (in both magnitude and form) but the correspondence is not mirrored in the behaviour of the two sets of apparent resistivities. These differences would, in practice, make a combined interpretation across the three profiles difficult.

In contrast to 1-D modelling and inversion of VLF data (Mathieson and Crossley, 1982), 2-D modelling and inversion requires the appropriate mode of the data to be established. The choice of whether the observed data are responding in either the TE-mode or TM-mode will inevitably be subject to error unless an unambiguous anomaly strike direction is known and measurements are then made using VLF transmitters in principal strike coordinates (i.e. perpendicular and/or parallel to strike). Even in the case, as here, where a small topographic feature at the surface is thought to relate (in some unknown way) to the fault at depth, it should be noted that the VLF wavefield at 16 kHz may effectively respond to resistivity gradients to a considerable depth (e.g. $>$ 20 metres).

A great deal of insight into the procedure for establishing the correct mode of the data can be obtained using the response characteristics of synthetic models such as those presented in the previous sections. Referring to Figure 5 (synthetic example 2), both the TE- and TM-mode responses in apparent resistivity display minima in the vicinity of the resistivity contrast. In such a case (i.e. a conductive anomaly) the TM-mode phase will display a characteristic increase (to a maximum) while the TE-mode phase displays a corresponding decrease to provide a minimum. Thus the phase information can be diagnostic of the induction mode. In this case we can compare the synthetic TE- and TM-mode phase response (Figure 5) with that of the observed data (Figures 12 to 14). In Figures 12 and 13 it can be seen that phase maxima are observed on profiles 00S and 10S in association with minima in the amplitude responses and as such should be associated with a TM-mode response. The phase behaviour along profile 20S, although less convincing, is still compatible with TM-mode behaviour.

The Z field data, when available, can provide an additional constraint with regard to mode identification. A Z-field can only be generated in the case of a TE-mode response. It is entirely absent in the case of pure TM-mode induction (under the 2-D assumption). The Z field response observed in the TE-mode across the second synthetic model was shown in Figure 6. Here it can be noted that the in-phase response changes sign at the location where the minima in apparent resistivities are observed. Maxima and minima in the Z-field are then observed to either side of the phase change. The essential point is that in the case of a TE-mode response which gives rise to a significant lateral VLF-R response, an associated VLF-Z response must always exist.

In the case of the present survey data, the measured VLF-Z response is limited to values < 0.07 (Fig. 11). This fact, together with the characteristic VLF-R phase behaviour noted above confirms that the measured data conform, quite closely, to a TM-mode response.

Using the data shown by symbols in Figures 12 to 14, a series of investigations into the resistivity cross-sections were made using the 2-D OCCAM algorithm, under the assumption that the data represent a TM-mode response. As in the previous synthetic examples, a 'blind' starting model of 30 ohm.m was used in each case. Using the nominal 2.5% error assignments, it was found that the data from all three profiles could be inverted in one or two iterations to provide an r.m.s. misfit of unity. The responses of the models obtained by this procedure are shown by the broken lines in Figures 12 to 14.

The three resistivity cross-sections obtained are shown in Figures 15 (profile 00S), 16 (profile 10S) and 17 (profile 20S). All three cross-sections display smooth resistivity transitions between 'conductive' regions of order 25 ohm.m through to more resistive regions with resistivities > 100 ohm.m. The cross-sections obtained for profiles 10S and 20S (Figures 16 and 17) show a similar form i.e. a near-surface resistivity low centred on -155 in Figure 16, transfers to a more westerly (i.e. to the left) position in Figure 17. In the case of profile 00S (Fig. 15) the near-surface conductive feature is centred on -140 and the cross-section involves less steeply-dipping gradients.

Resolution in minimum-structure inversion is a function of misfit. An examination of the model fits obtained at unity misfit (Figures 12 to 14) indicates that, particularly in the case of the phase data, the lower-order data wavelengths have only been partially reproduced. We could, in fact, regard the cross-sections associated with these fits as 'conservative' estimates of the most likely resistivity distribution. The OCCAM algorithm is, in general, capable of providing a cross-section that fits most of the fine-detail of valid observational data. With decreasing misfit, however, we must eventually start to model noise.

The observational data can be viewed as containing a superposition of wavenumber components. The fitting of the low wavenumber components to an r.m.s. misfit of unity provided the cross-sections which can be seen to contain only long wavelength gradients. High-wavenumber features in the data (e.g. gradients at the measurement separation scale) can only be modelled by short-wavelength features in the cross-section. In cases where such gradients are 'noise', artificial model features, particularly in the shallow sub-surface, will inevitably be produced.

These points are well-demonstrated by the three data sets considered here. Figures 18 to 20 show the three resistivity cross-sections obtained by reducing the misfit level to 0.25 (with assumed data errors remaining at 2.5%). The associated response data are compared with the observed data by the solid lines in Figures 12 to 14. Here it can be seen that a degree of 'overfit' has taken place in providing models which fit the data 'exactly'. The cross-sections

now contain some high-wavenumber features which, particularly within the upper 10 m, are most likely to be 'noise'. Some of the lower wavenumber features are, however, stable developments of features observed previously at the lower level of misfit.

For the data sets considered here, the most realistic cross-sections lie within the 'limits' provided by the two sets of results (i.e. at misfits of 1 and 0.25). Both sets can be used for interpretation purposes with the 0.25 level results requiring a much higher degree of caution. It can be noted from Figures 18 and 19 that the characteristic dipping conductive feature is compatible with that imaged in the second synthetic model analysis. The previous (forward) model analyses therefore represent an important aspect of interpretation control. The results from the southern-most profile 20S (Fig. 20) do not preclude the same type of feature. In the case of 20S, the same (assumed) feature appears to lie too close to the edge of the observational profile to allow the 'same degree' of resolution.

Using the synthetic model results as a control, the interpretation of features observed in the resistivity cross-sections can be undertaken. A subsurface conductive zone, assumed to be fault-related, occurs on all three cross-sections. The lowest resistivity within the zone (averaged over 2.5 x 2.5 m) is of the order of 15 to 20 ohm.m. Away from the immediate vicinity of this zone at- and near-surface resistivities return to values in excess of 100 ohm.m. The upper surface of the zone lies some 3 to 5 m beneath the surface.

On profiles 00S and 10S the position of the upper surface of the conductive zone lies directly beneath a previously identified topographic feature. The resolution of (possibly) the same zone on profile 20S is made difficult due to the lateral limits of the observations. On profiles 00S and 10S the conductive feature has a strong component of dip that probably exceeds 45 degrees in both cases. Using observations at 5 m separations, our resolution of the true width of the zone is limited. Although the intrinsic resolution through the deeper part of the section is poor, on the basis of the control model results, it is possible to suggest that the conductive feature maintains a significant resistivity contrast only to depths of the order of 20 to 30 m.

Conclusions.

VLF-EM observations (both VLF-Z and VLF-R) provide profile information which usually require to be modelled by a 2-D cross-section of resistivity structure. Viewed from the perspective of other, multi-frequency EM techniques the VLF method is a high-density but essentially single-frequency method. These characteristics present data modelling techniques, particularly that of data inversion, with a special case of observational insufficiency.

The 2-D data modelling described here imposes additional demands on the procedures of directional VLF data acquisition (to avoid inconsistency with the 2-D approach). Where geological strike is not known, measurements need to be made using two or more azimuthally-distinct transmitters.

The application of a 2-D regularised inversion scheme, to both synthetic and field data, has demonstrated that the inherent data insufficiency can be compensated, to some degree, by imposing the constraint of minimum-structure. Regularised inversion schemes are capable of the automatic construction of credible resistivity models. The results demonstrate that the resistivity gradients contained in such models must still be interpreted with care. A single frequency EM technique can only provide a limited vertical resolution. The synthetic studies indicate that the zone of first wavefield contact with an anomalous region produces the highest level of structural resolution. Beneath this region, with increasing depth, resolution must inevitably decrease. Forward resolution studies of type-examples, to clarify the interpretation of inverted field data, are recommended.

Acknowledgements.

The research was funded in part by the Commission of the European Communities. The report is published with the approval of the Director, British Geological Survey (NERC).

References.

Constable, S.C., Parker, R.L. and Constable, C.G., 1987. Occam's inversion : a practical algorithm for generating smooth models from EM sounding data. Geophysics, **92**, 289-300.

deGroot-Hedlin, C.M. and Constable, S.C., 1990. Occam's inversion to generate smooth, two-dimensional models from magnetotelluric data. Geophysics, **55**, 1613-1624.

Fischer, G., Le Quang, B.V. and Muller, I., 1983. VLF ground surveys, a powerful tool for the study of shallow two-dimensional structures. Geophys. Prosp., **31**, 977-991.

Greenwood, P.G. and Peart, R.G., 1992. Methods for recognition of geological weakness zones and other surface discontinuities caused by underground mining in Carboniferous terrain. British Geological Survey Technical Report WN/93/02C.

Jackson, D.D., 1972. Interpretation of inaccurate, insufficient and inconsistent data. Geophys. J. R. astr. Soc., **28**, 97-110.

Mathieson, C. and Crossley, D.J., 1981. Interpretation of single frequency VLF data. In : L.S. Collett and O.G. Jenson (Editors), Geophysical Applications of Surface Wave Impedance Measurements, Geological Survey of Canada, Paper 81-15, pp. 49-65.

McNeill, J.D., 1990. Use of electromagnetic methods for groundwater studies. In : S.H. Ward (Editor), Geotechnical and Environmental Geophysics, Vol. 1 : Review and Tutorial. SEG, Tulsa, OK, pp. 191-218.

Ogilvy, R.D., Cuadra, A., Jackson, P.D. and Monte, J.L., 1991. Detection of an air-filled drainage gallery by the VLF resistivity method. Geophys. Prosp., **39**, 845-859.

Parker, R.L. and Whaler, K.A., 1981. Numerical methods for establishing solutions to the inverse problem of electromagnetic induction. J. Geophys. Res., **86**, 9574-9584.

Smith, J.T. and Booker, J.R., 1988. Magnetotelluric inversion for minimum structure. Geophysics, **53**, 1565-1576.

Smith, J.T. and Booker, J.R., 1991. Rapid inversion of two- and three-dimensional magnetotelluric data. J. Geophys. Res., **96**, 3905-3922.

Strangway, D.W., Swift, Jr, C.M. and Holmer, R.C., 1973. The application of audio-frequency magnetotellurics (AMT) to mineral exploration. Geophysics, **38**, 1159-1175.

Tabbagh, A., Benderitter, Y., Andrieux, P., Decriaud, J.P. and Guerin, R., 1991. VLF resistivity mapping and verticalization of the electric field. Geophys. Prosp., **39**, 1083-1097.

Wannamaker, P.E., Stodt, J.A. and Rijo, L., 1987. A stable finite element solution for two-dimensional magnetotelluric modelling. Geophys. J. R. astr. Soc., **88**, 277-296.

Figure Captions.

Figure 1. Response of synthetic model 1 at 16 kHz (solid circle symbols) and 25 kHz (open cross symbols) at 11 locations (-175 to -125 metres). Error bars denote 1% error bounds assigned. Solid lines are inversion model results discussed in the text. Apparent resistivity, on logarithmic scale (upper diagram), phase (lower diagram).

Figure 2. Smooth resistivity solution obtained by inverting the TE-mode data at 16 kHz of synthetic model 1. The r.m.s. misfit is unity. The model is shown outlined by the heavy dashed line. Results contoured are the logarithm of the resistivity using a contour interval of 0.25 (except for lowest bound). The blank (white) zone corresponds to modelled resistivities < 5 ohm.m. True scale cross-section.

Figure 3. Smooth resistivity solution obtained by inverting the TE-mode data at two frequencies of 16 and 25 kHz of synthetic model 1. The r.m.s. misfit is unity. The model is shown outlined by the heavy dashed line. Results contoured are the logarithm of the resistivity using a contour interval of 0.25 (except for lowest bound). The blank (white) zone corresponds to modelled resistivities < 5 ohm.m. True scale cross-section.

Figure 4. Smooth resistivity solution obtained by inverting the TE-mode data at two frequencies of 16 and 25 kHz of synthetic model 1. The r.m.s. misfit is 0.5. The model is shown outlined by the heavy dashed line. Results contoured are the logarithm of the resistivity using a contour interval of 0.25 (except for lowest bound). The blank (white) zone corresponds to modelled resistivities < 5 ohm.m. True scale cross-section.

Figure 5. VLF-R response of synthetic model 2 at 16 kHz, TE-mode (joined solid circles), TM-mode (joined open crosses) at 11 locations (-175 to -125 metres). Error bars (1% error bounds) are less than size of symbols. Apparent resistivity, on logarithmic scale (upper diagram), phase (lower diagram).

Figure 6. VLF-Z response of synthetic model 2 at 16 kHz, TE-mode. In-phase component (solid circles), in-quadrature component (open crosses) at 11 locations (-175 to -125 metres). Error bars (1% error bounds) are less than size of symbols.

Figure 7. Smooth resistivity solution obtained by inverting the TE-mode data (VLF-R) at a frequency of 16 kHz for synthetic model 2. The r.m.s. misfit is 1.0. The model is shown outlined by the heavy dashed line. Results contoured are the logarithm of the resistivity using a contour interval of 0.25. True scale cross-section.

Figure 8. Smooth resistivity solution obtained by inverting the TM-mode data (VLF-R) at a frequency of 16 kHz for synthetic model 2. The r.m.s. misfit is 1.0. The model is shown outlined by the heavy dashed line. Results contoured are the logarithm of the resistivity using a contour interval of 0.25. True scale cross-section.

Figure 9. Smooth resistivity solution obtained by inverting the TE-mode data (VLF-R and VLF-Z) at a frequency of 16 kHz for synthetic model 2. The r.m.s. misfit is 1.0. The model is shown outlined by the heavy dashed line. Results contoured are the logarithm of the resistivity using a contour interval of 0.25. True scale cross-section.

Figure 10. Smooth resistivity solution obtained by inverting the TM-mode data (VLF-R) at a two frequencies of 16 and 25 kHz for synthetic model 2. The r.m.s. misfit is 1.0. The model is shown outlined by the heavy dashed line. Results contoured are the logarithm of the resistivity using a contour interval of 0.25. True scale cross-section.

Figure 11. Plan view of three profiles of VLF measurements. The three profiles are referred to as 00S, 10S and 20S. The ? fault trace is a 10 cm topographic feature. The results contoured are the VLF-Z in-phase component expressed as a percentage.

Figure 12. VLF-R data along profile 00S. The solid symbols are the observed data. Error bars are 2.5% error bounds. The connecting lines are inversion model results. Dashed line (r.m.s. misfit of 1.0), full line (r.m.s. misfit of 0.25).

Figure 13. VLF-R data along profile 10S. The solid symbols are the observed data. Error bars are 2.5% error bounds. The connecting lines are inversion model results. Dashed line (r.m.s. misfit of 1.0), full line (r.m.s. misfit of 0.25).

Figure 14. VLF-R data along profile 20S. The solid symbols are the observed data. Error bars are 2.5% error bounds. The connecting lines are inversion model results. Dashed line (r.m.s. misfit of 1.0), full line (r.m.s. misfit of 0.25).

Figure 15. Profile 00S, r.m.s = 1.0. Smooth resistivity solution obtained by inverting VLF-R data along 00S. The r.m.s. misfit is 1.0. Results contoured are the logarithm of the resistivity using a contour interval of 0.1. True scale cross-section.

Figure 16. Profile 10S, r.m.s = 1.0. Smooth resistivity solution obtained by inverting VLF-R data along 10S. The r.m.s. misfit is 1.0. Results contoured are the logarithm of the resistivity using a contour interval of 0.1. True scale cross-section.

Figure 17. Profile 20S, r.m.s = 1.0. Smooth resistivity solution obtained by inverting VLF-R data along 20S. The r.m.s. misfit is 1.0. Results contoured are the logarithm of the resistivity using a contour interval of 0.1. True scale cross-section.

Figure 18. Profile 00S, r.m.s = 0.25. Smooth resistivity solution obtained by inverting VLF-R data along 00S. The r.m.s. misfit is 0.25. Results contoured are the logarithm of the resistivity using a contour interval of 0.1. True scale cross-section.

Figure 19. Profile 10S, r.m.s = 0.25. Smooth resistivity solution obtained by inverting VLF-R data along 10S. The r.m.s. misfit is 1.0. Results contoured are the logarithm of the resistivity using a contour interval of 0.1. True scale cross-section.

Figure 20. Profile 20S, r.m.s = 0.25. Smooth resistivity solution obtained by inverting VLF-R data along 20S. The r.m.s. misfit is 1.0. Results contoured are the logarithm of the resistivity using a contour interval of 0.1. True scale cross-section.

Figure 1

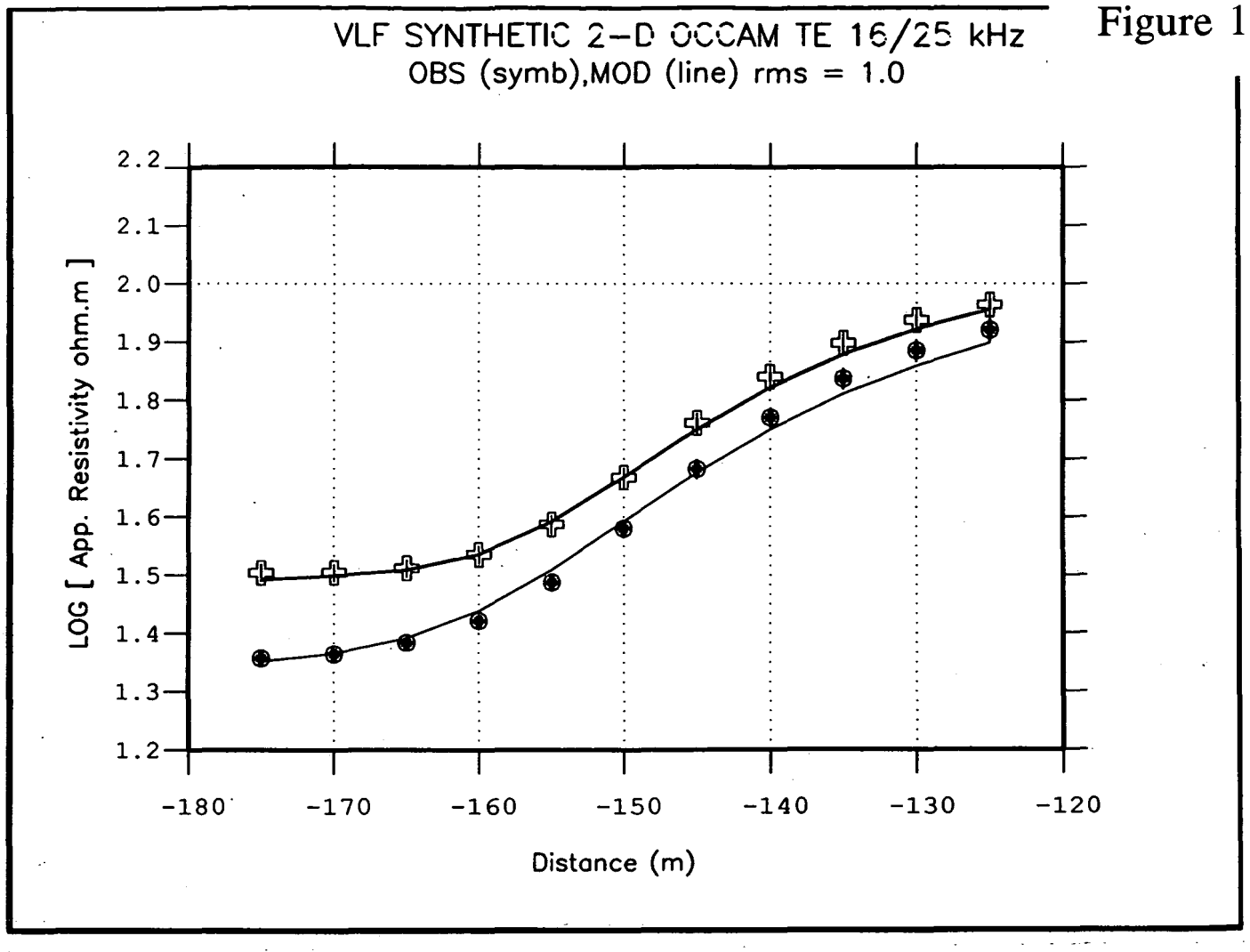
VLF SYNTHETIC 2-D OCCAM TE 16/25 kHz
OBS (symb),MOD (line) rms = 1.0
LOG [App. Resistivity ohm.m]
2.2
2.1
2.0
1.9
1.8
1.7
1.6
1.5
1.4
1.3
1.2
-180
-170
-160
-150
-140
-130
-120
Distance (m)

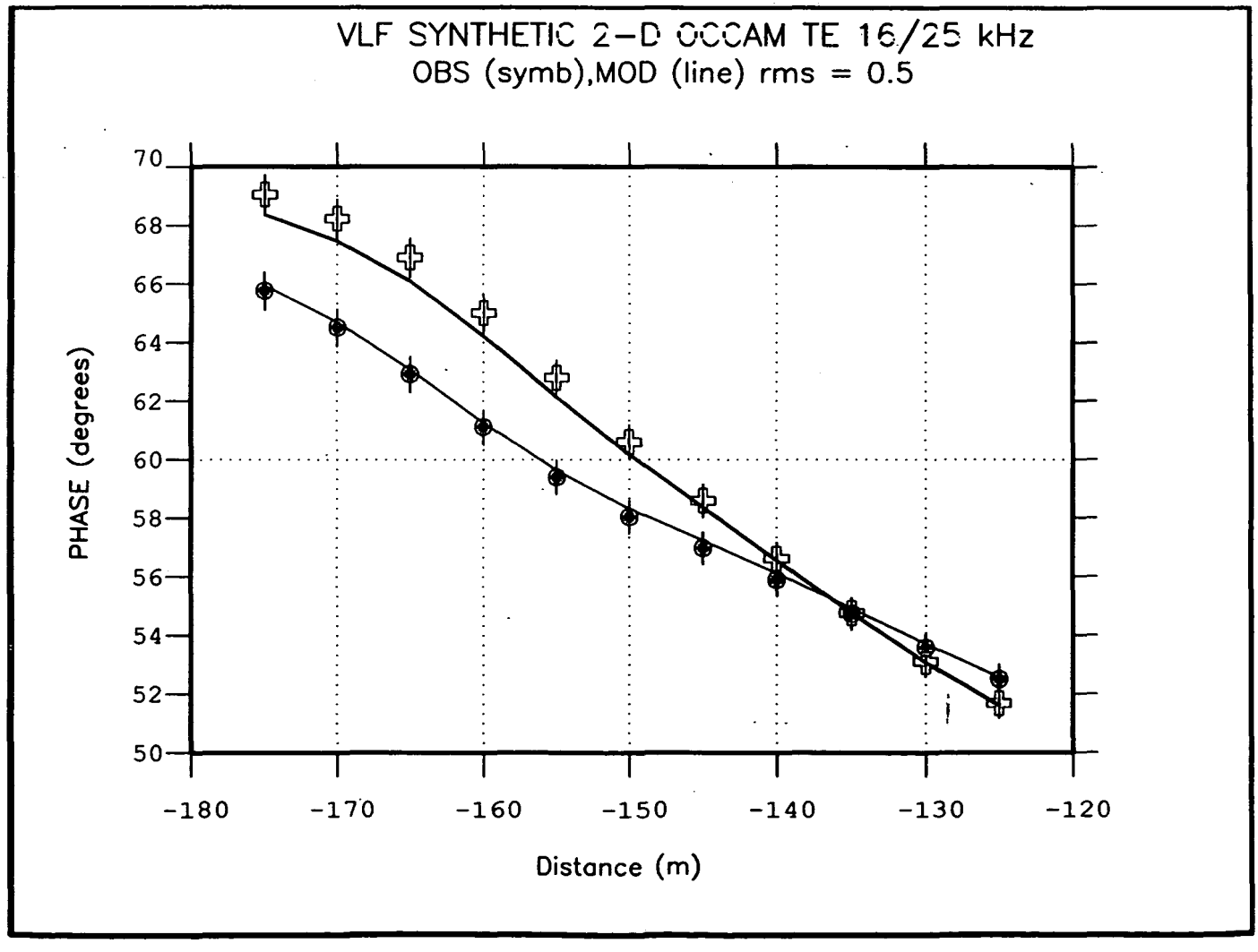
VLF SYNTHETIC 2-D OCCAM TE 16/25 kHz
OBS (symb),MOD (line) rms = 0.5
PHASE (degrees)
70
68
66
64
62
60
58
56
54
52
50
-180
-170
-160
-150
-140
-130
-120
Distance (m)

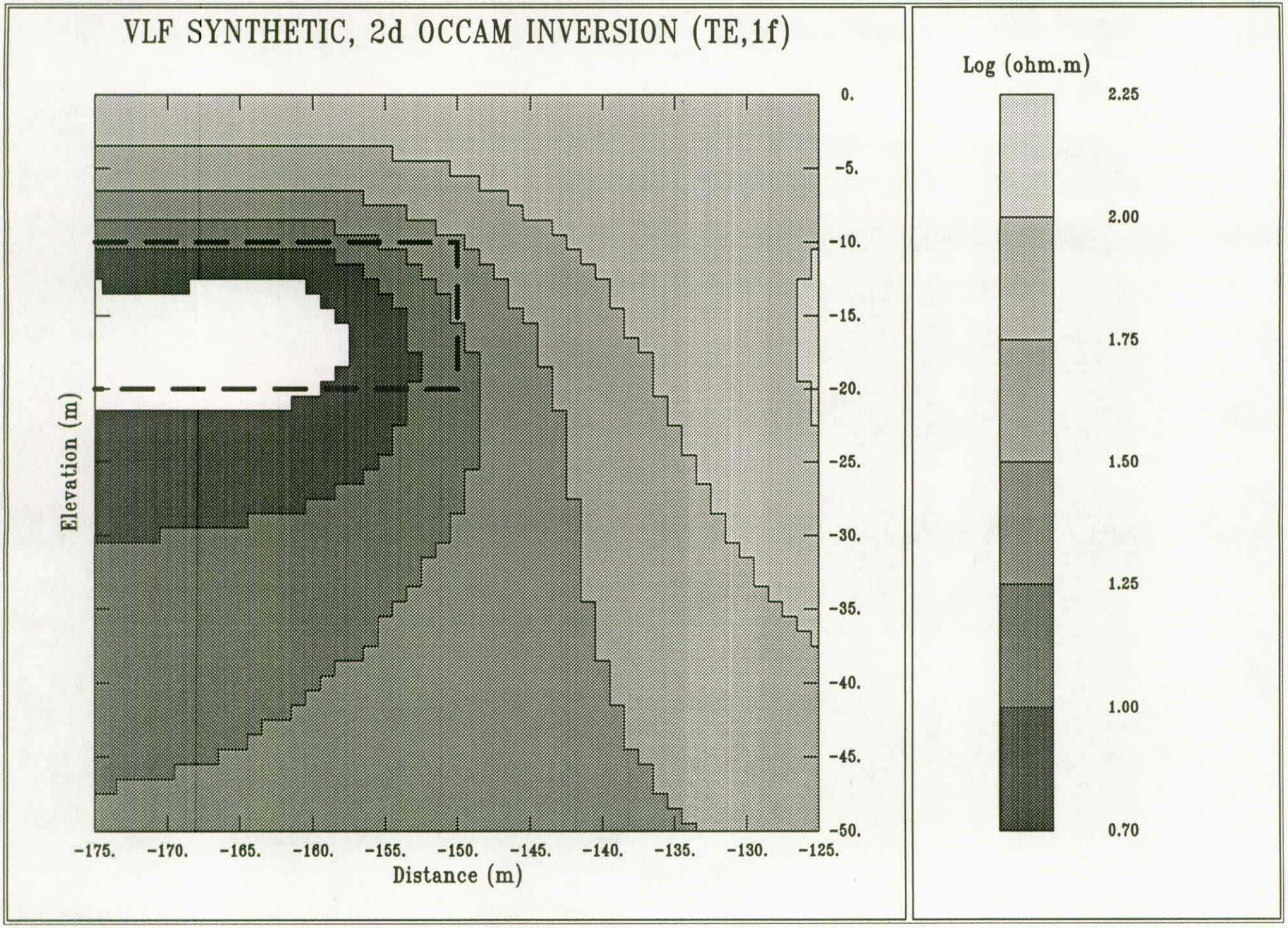
VLF SYNTHETIC, 2d OCCAM INVERSION (TE,1f)
Elevation (m)
0.
-5.
-10.
-15.
-20.
-25.
-30.
-35.
-40.
-45.
-50.
-175.
-170.
-165.
-160.
-155.
-150.
-145.
-140.
-135.
-130.
-125.
Distance (m)
Log (ohm.m)
2.25
2.00
1.75
1.50
1.25
1.00
0.70

Figure 2

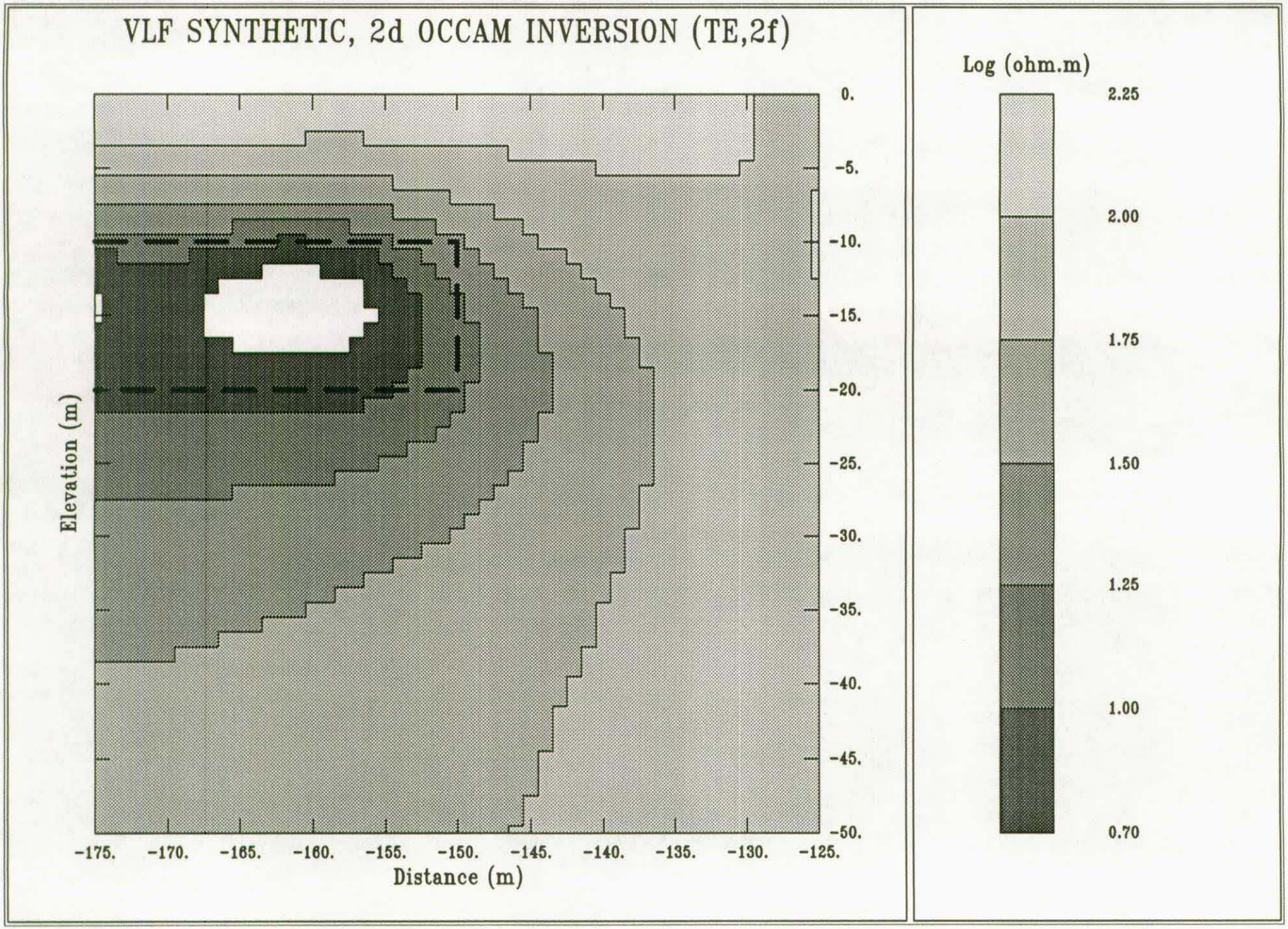
VLF SYNTHETIC, 2d OCCAM INVERSION (TE,2f)
Elevation (m)
0.
-5.
-10.
-15.
-20.
-25.
-30.
-35.
-40.
-45.
-50.
-175.
-170.
-165.
-160.
-155.
-150.
-145.
-140.
-135.
-130.
-125.
Distance (m)
Log (ohm.m)
2.25
2.00
1.75
1.50
1.25
1.00
0.70

Figure 3

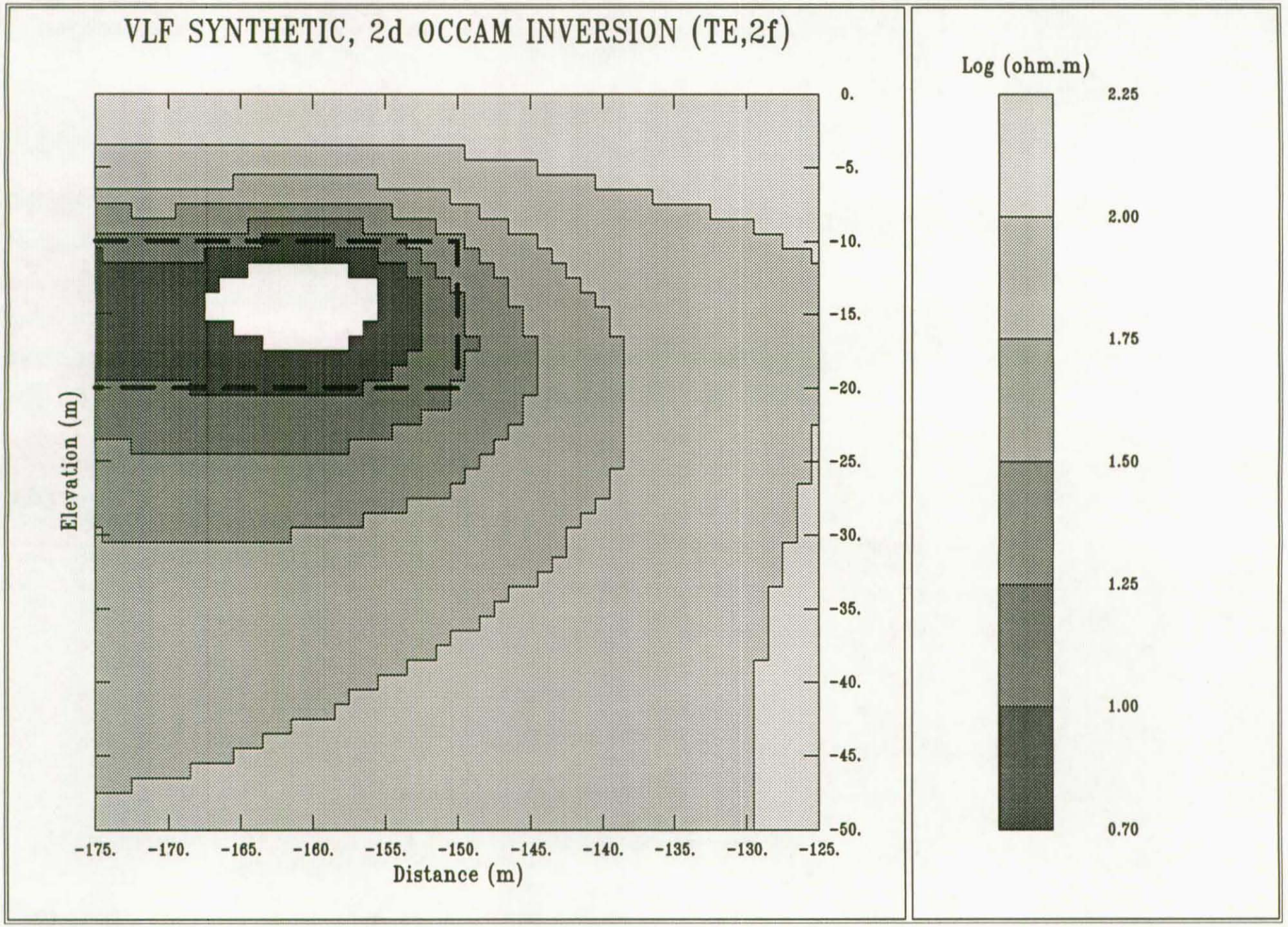
VLF SYNTHETIC, 2d OCCAM INVERSION (TE,2f)
Elevation (m)
0.
-5.
-10.
-15.
-20.
-25.
-30.
-35.
-40.
-45.
-50.
-175.
-170.
-165.
-160.
-155.
-150.
-145.
-140.
-135.
-130.
-125.
Distance (m)
Log (ohm.m)
2.25
2.00
1.75
1.50
1.25
1.00
0.70

Figure 4

Figure 5

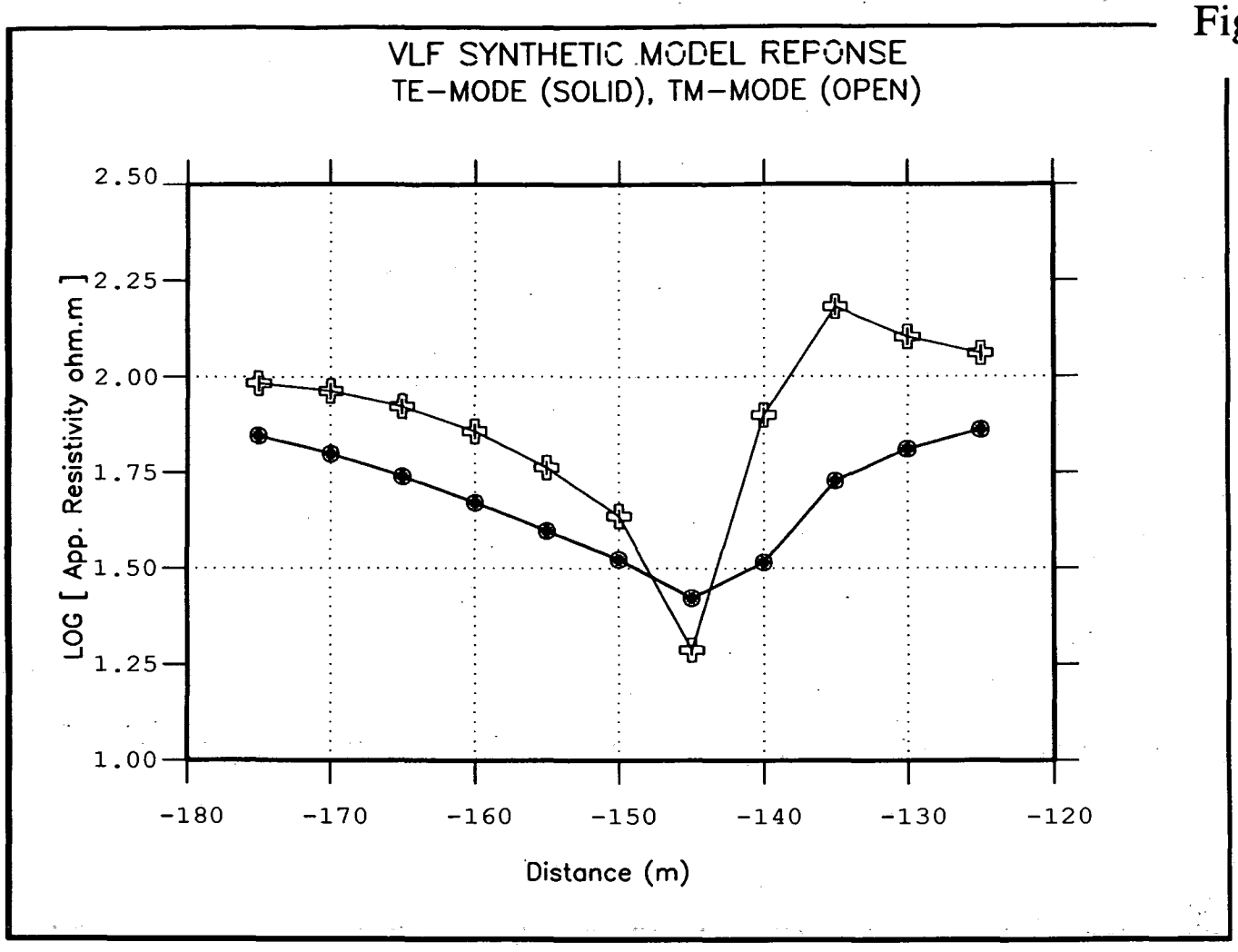
VLF SYNTHETIC MODEL REPONSE
TE-MODE (SOLID), TM-MODE (OPEN)
LOG [App. Resistivity ohm.m]
2.50
2.25
2.00
1.75
1.50
1.25
1.00
-180
-170
-160
-150
-140
-130
-120
Distance (m)

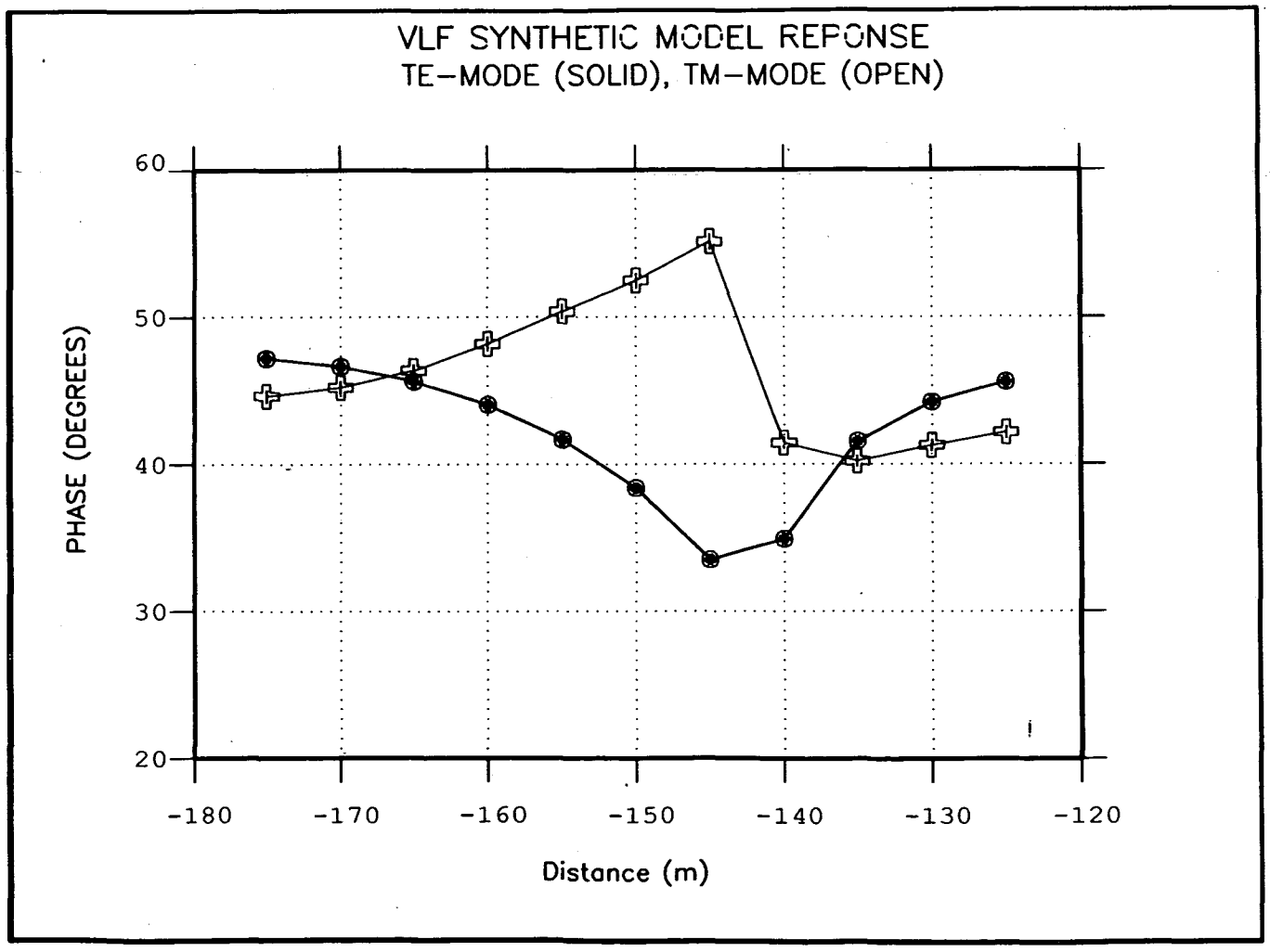
VLF SYNTHETIC MODEL REPONSE
TE-MODE (SOLID), TM-MODE (OPEN)
PHASE (DEGREES)
60
50
40
30
20
-180
-170
-160
-150
-140
-130
-120
Distance (m)

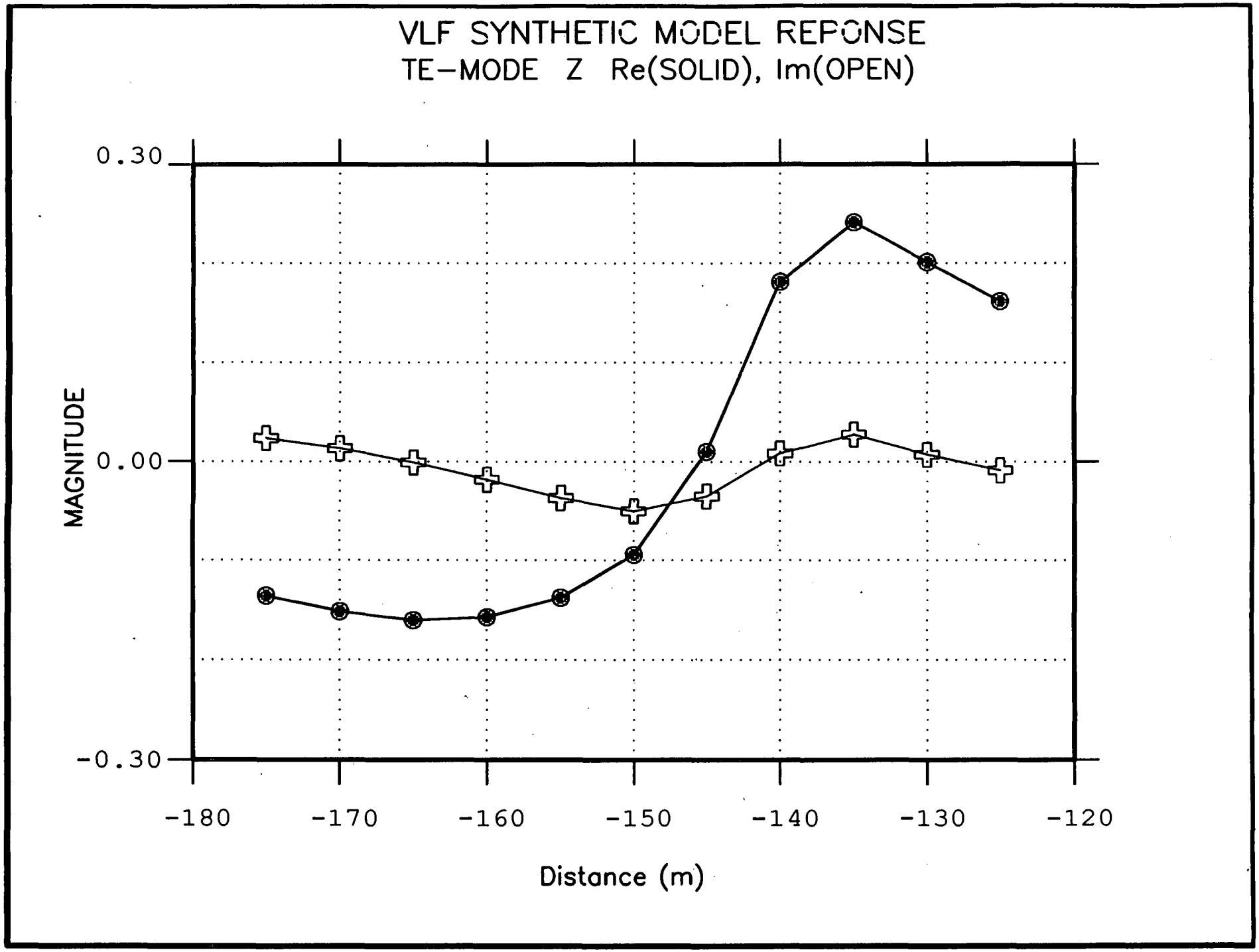
VLF SYNTHETIC MODEL REPONSE
TE-MODE Z Re(SOLID), Im(OPEN)
0.30
0.00
-0.30
MAGNITUDE
-180
-170
-160
-150
-140
-130
-120
Distance (m)

Figure 6

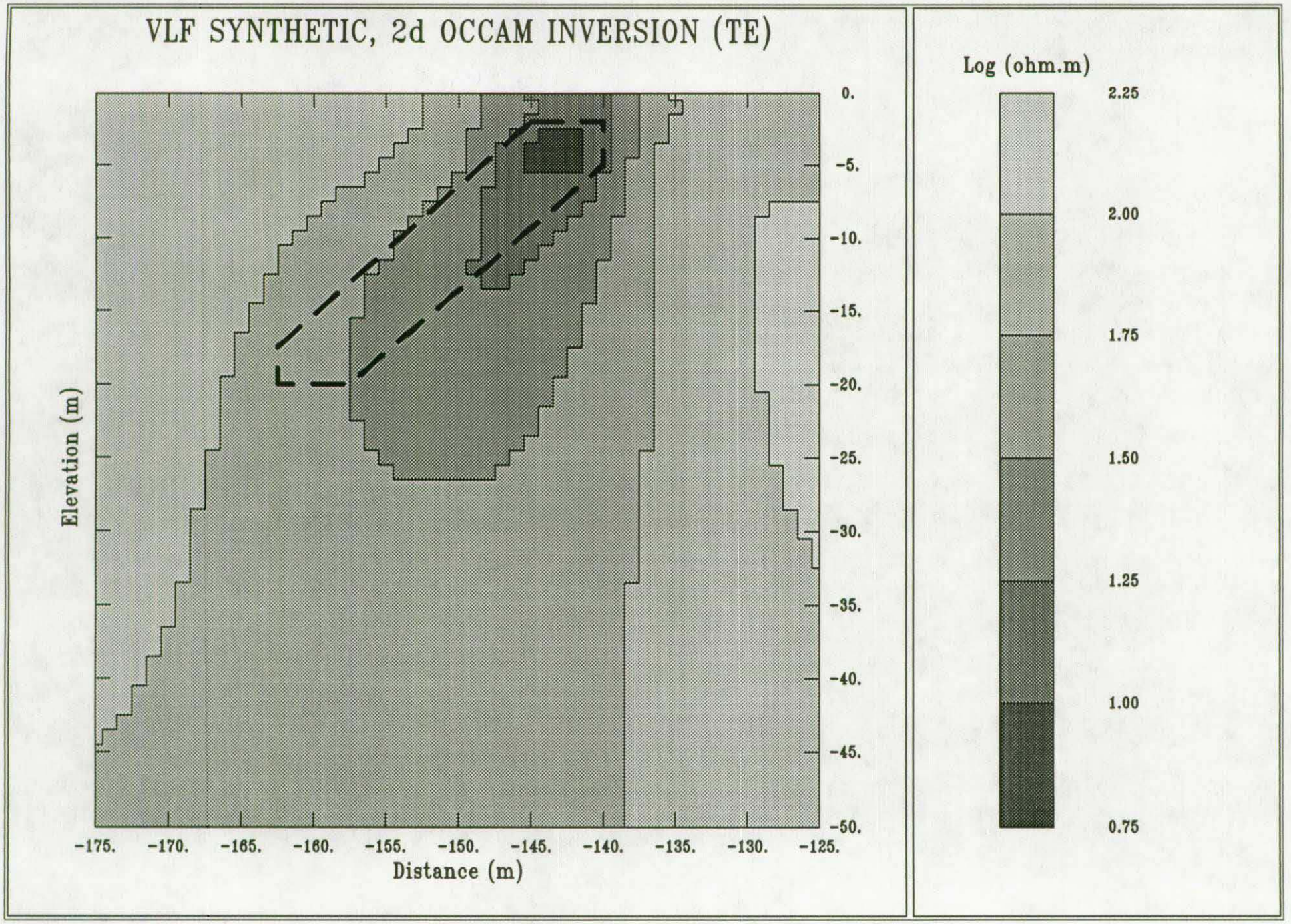
VLF SYNTHETIC, 2d OCCAM INVERSION (TE)
Elevation (m)
0.
-5.
-10.
-15.
-20.
-25.
-30.
-35.
-40.
-45.
-50.
-175.
-170.
-165.
-160.
-155.
-150.
-145.
-140.
-135.
-130.
-125.
Distance (m)
Log (ohm.m)
2.25
2.00
1.75
1.50
1.25
1.00
0.75

Figure 7

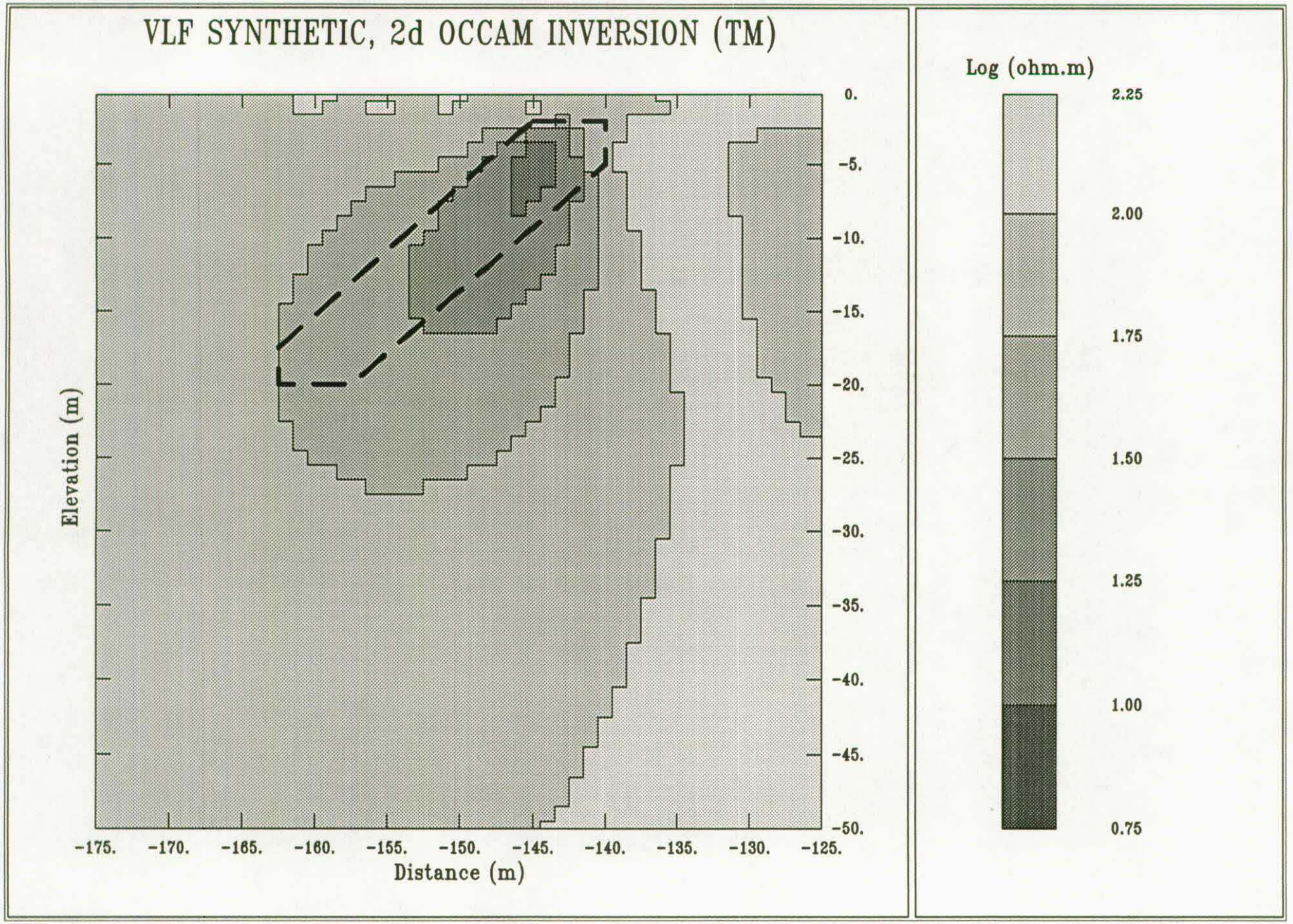
VLF SYNTHETIC, 2d OCCAM INVERSION (TM)
Elevation (m)
0.
-5.
-10.
-15.
-20.
-25.
-30.
-35.
-40.
-45.
-50.
-175.
-170.
-165.
-160.
-155.
-150.
-145.
-140.
-135.
-130.
-125.
Distance (m)
Log (ohm.m)
2.25
2.00
1.75
1.50
1.25
1.00
0.75

Figure 8

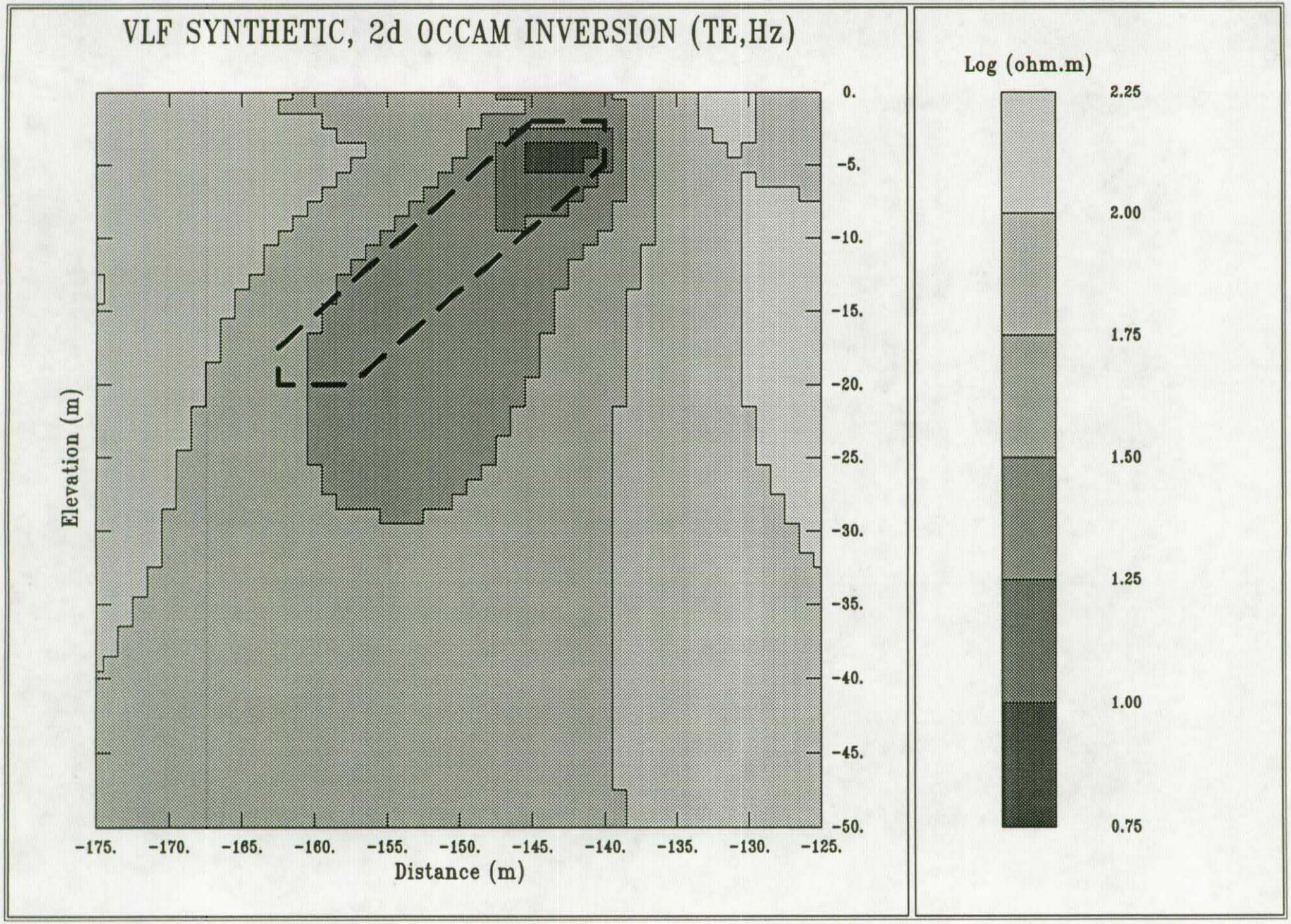
VLF SYNTHETIC, 2d OCCAM INVERSION (TE,Hz)
Elevation (m)
0.
-5.
-10.
-15.
-20.
-25.
-30.
-35.
-40.
-45.
-50.
-175.
-170.
-165.
-160.
-155.
-150.
-145.
-140.
-135.
-130.
-125.
Distance (m)
Log (ohm.m)
2.25
2.00
1.75
1.50
1.25
1.00
0.75

Figure 9

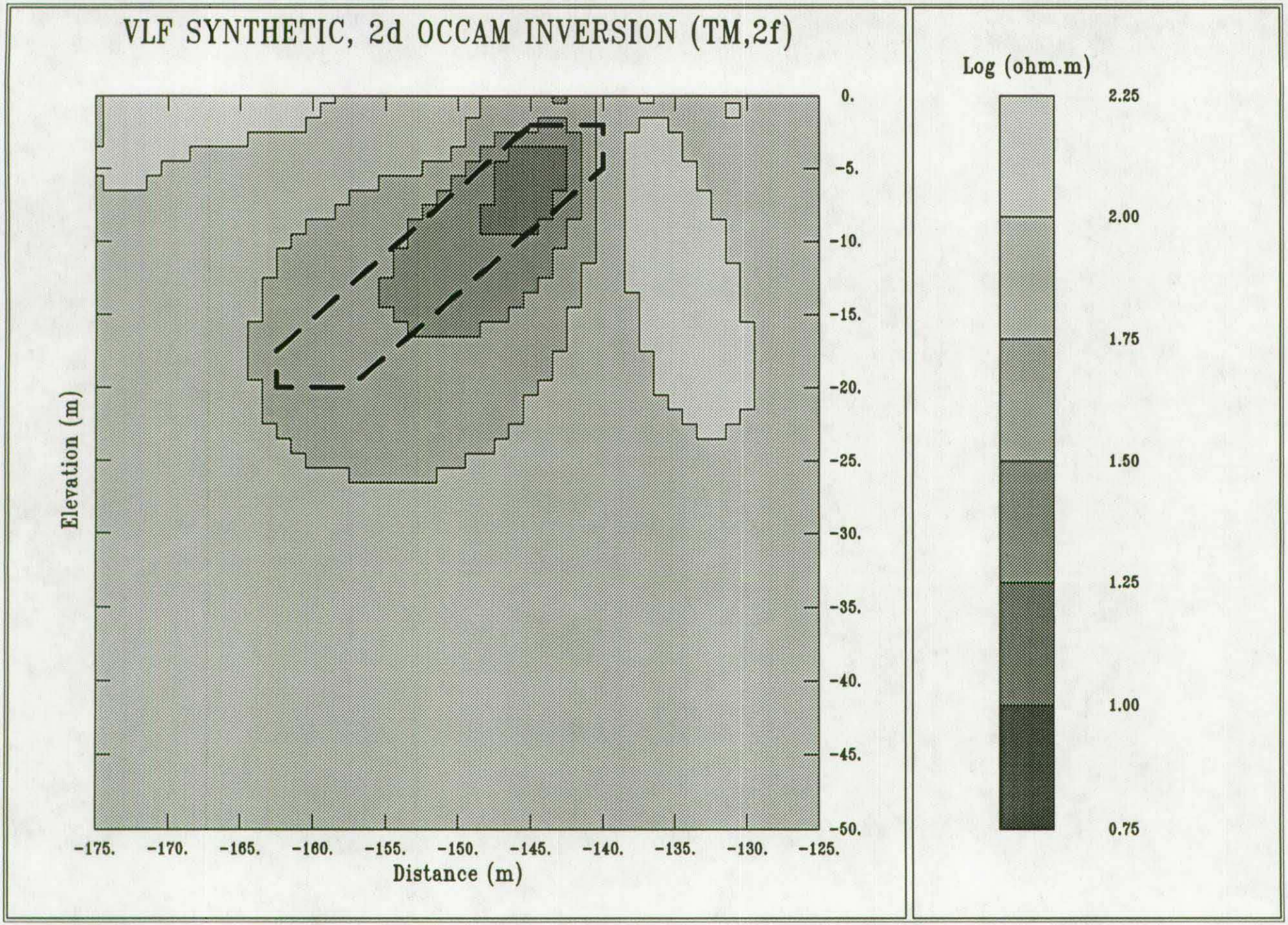
VLF SYNTHETIC, 2d OCCAM INVERSION (TM,2f)
Elevation (m)
0.
-5.
-10.
-15.
-20.
-25.
-30.
-35.
-40.
-45.
-50.
-175.
-170.
-165.
-160.
-155.
-150.
-145.
-140.
-135.
-130.
-125.
Distance (m)
Log (ohm.m)
2.25
2.00
1.75
1.50
1.25
1.00
0.75

Figure 10

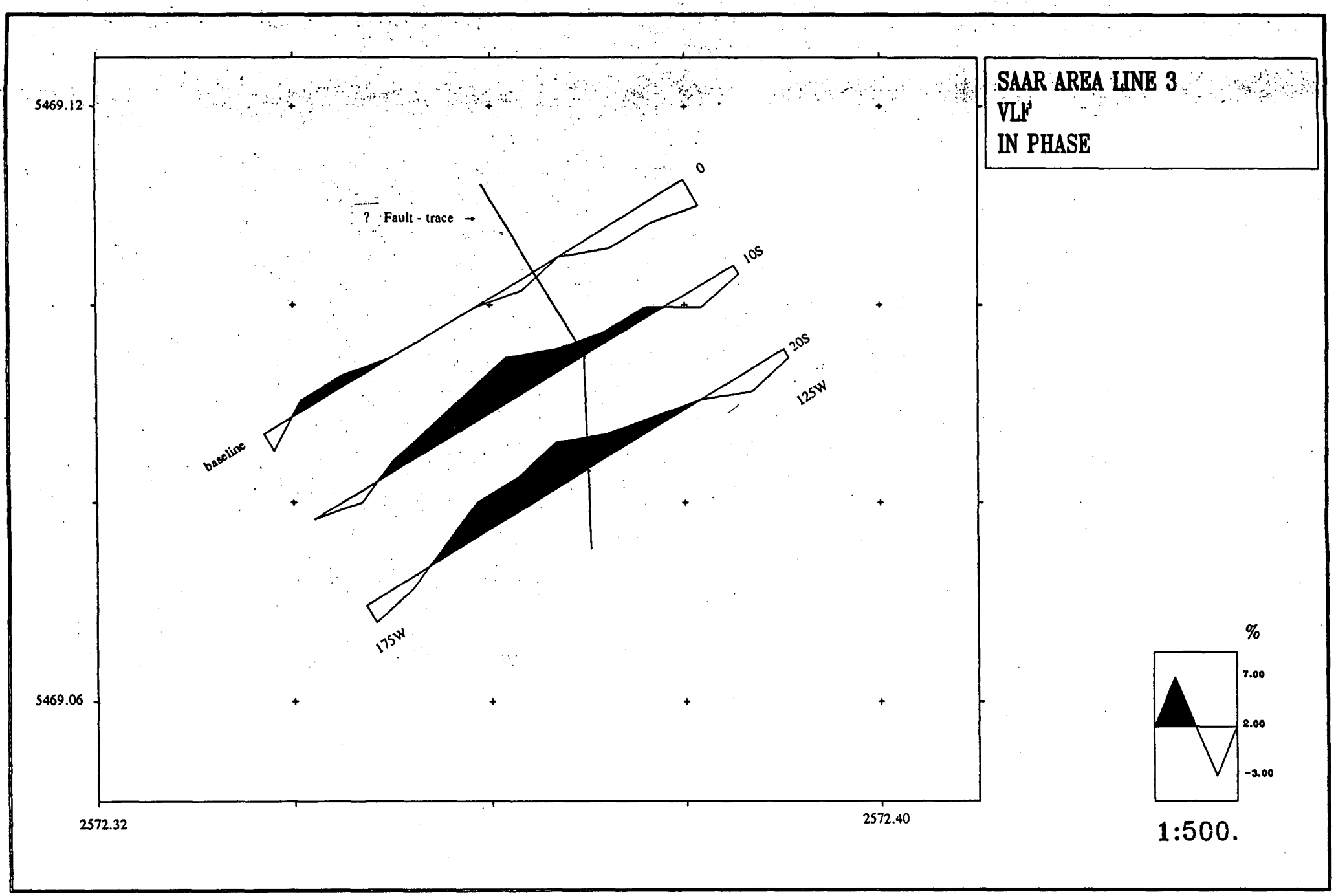
SAAR AREA LINE 3
VLF
IN PHASE
5469.12
5469.06
2572.32
2572.40
0
10S
20S
125W
175W
baseline
? Fault - trace →
%
7.00
2.00
-3.00
1:500.

Figure 11

Figure 12

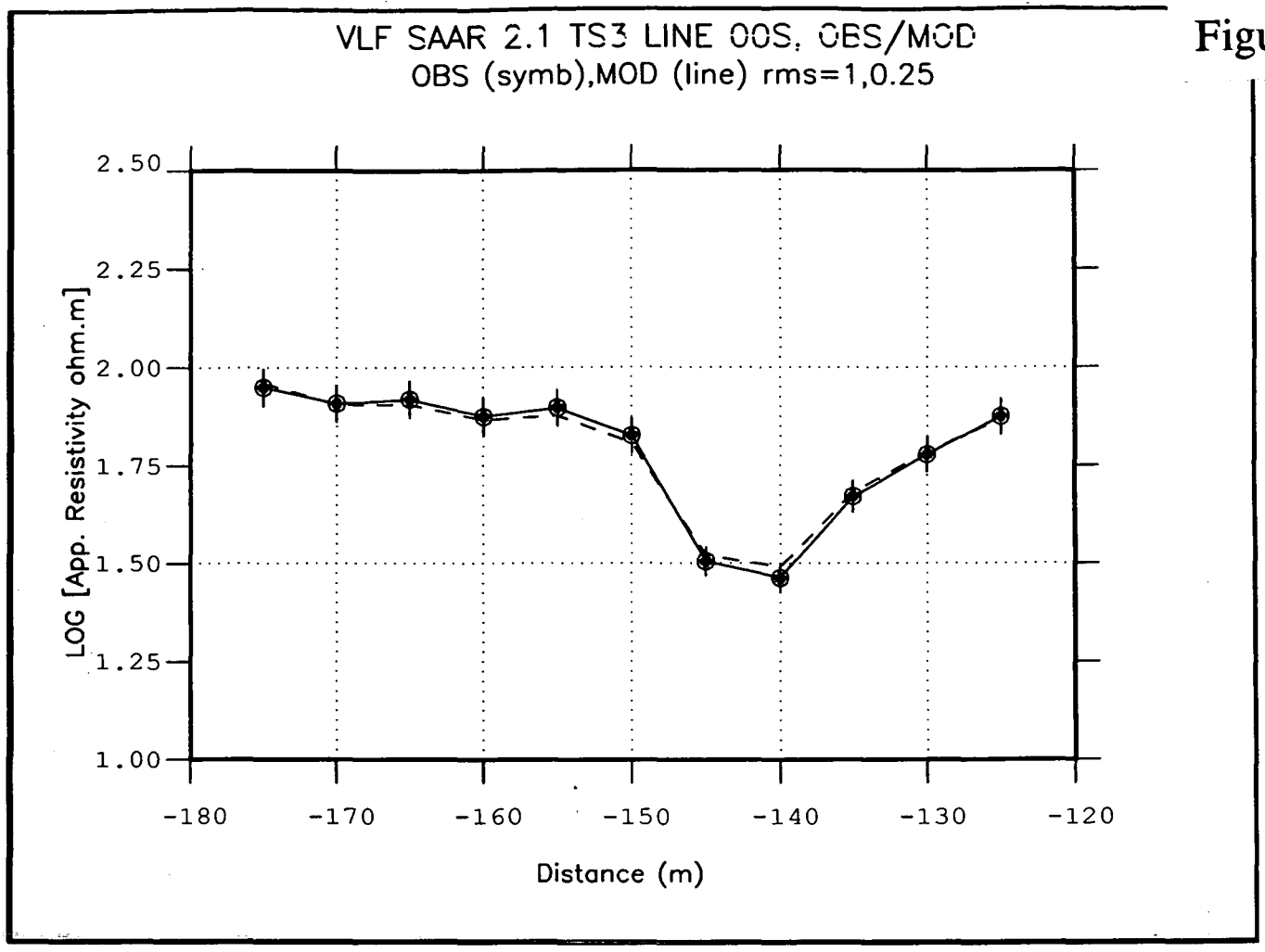
VLF SAAR 2.1 TS3 LINE 00S, OBS/MOD
OBS (symb),MOD (line) rms=1,0.25
LOG [App. Resistivity ohm.m]
2.50
2.25
2.00
1.75
1.50
1.25
1.00
-180
-170
-160
-150
-140
-130
-120
Distance (m)

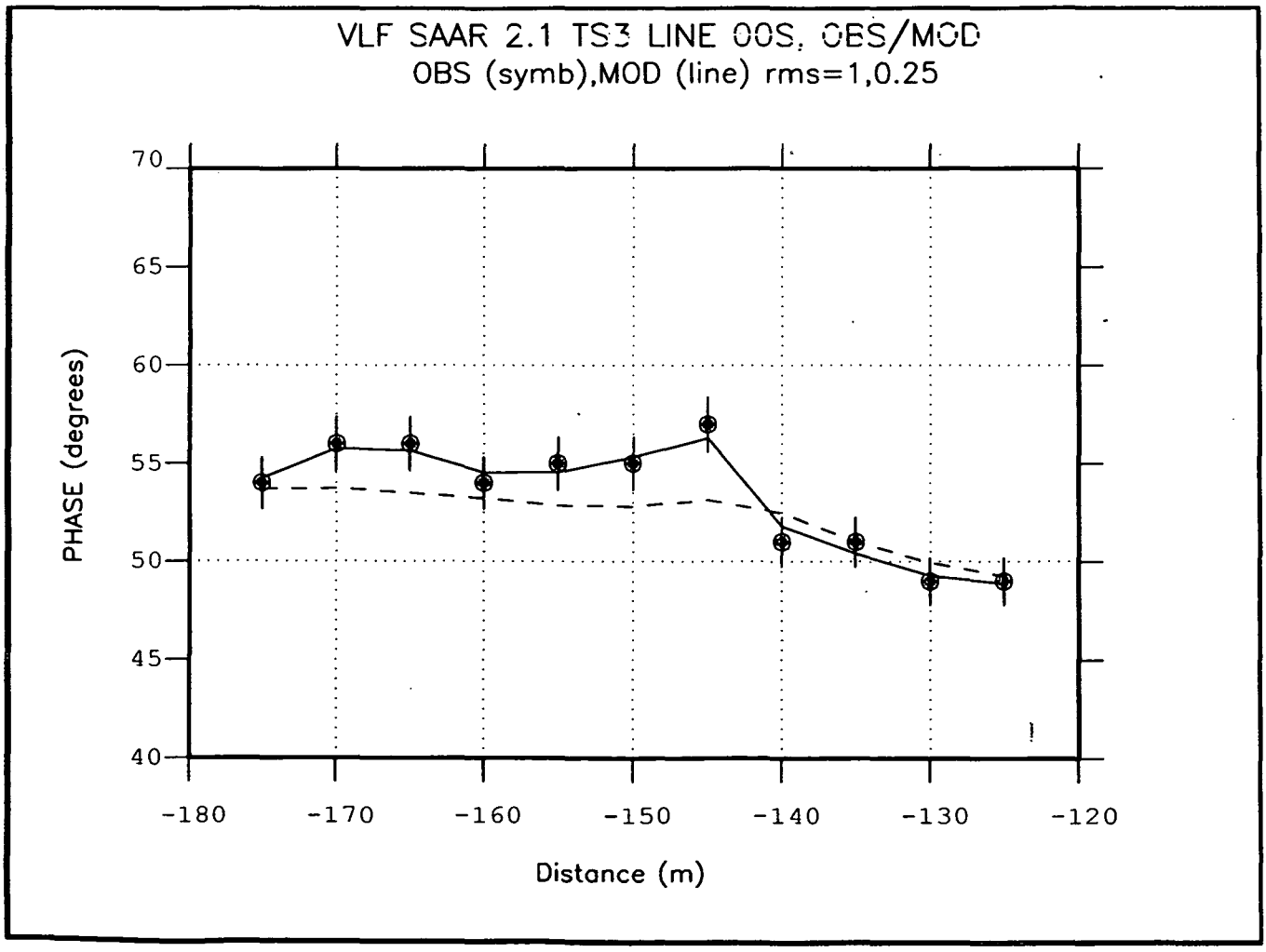
VLF SAAR 2.1 TS3 LINE 00S, OBS/MOD
OBS (symb),MOD (line) rms=1,0.25
PHASE (degrees)
70
65
60
55
50
45
40
-180
-170
-160
-150
-140
-130
-120
Distance (m)

Figure 13

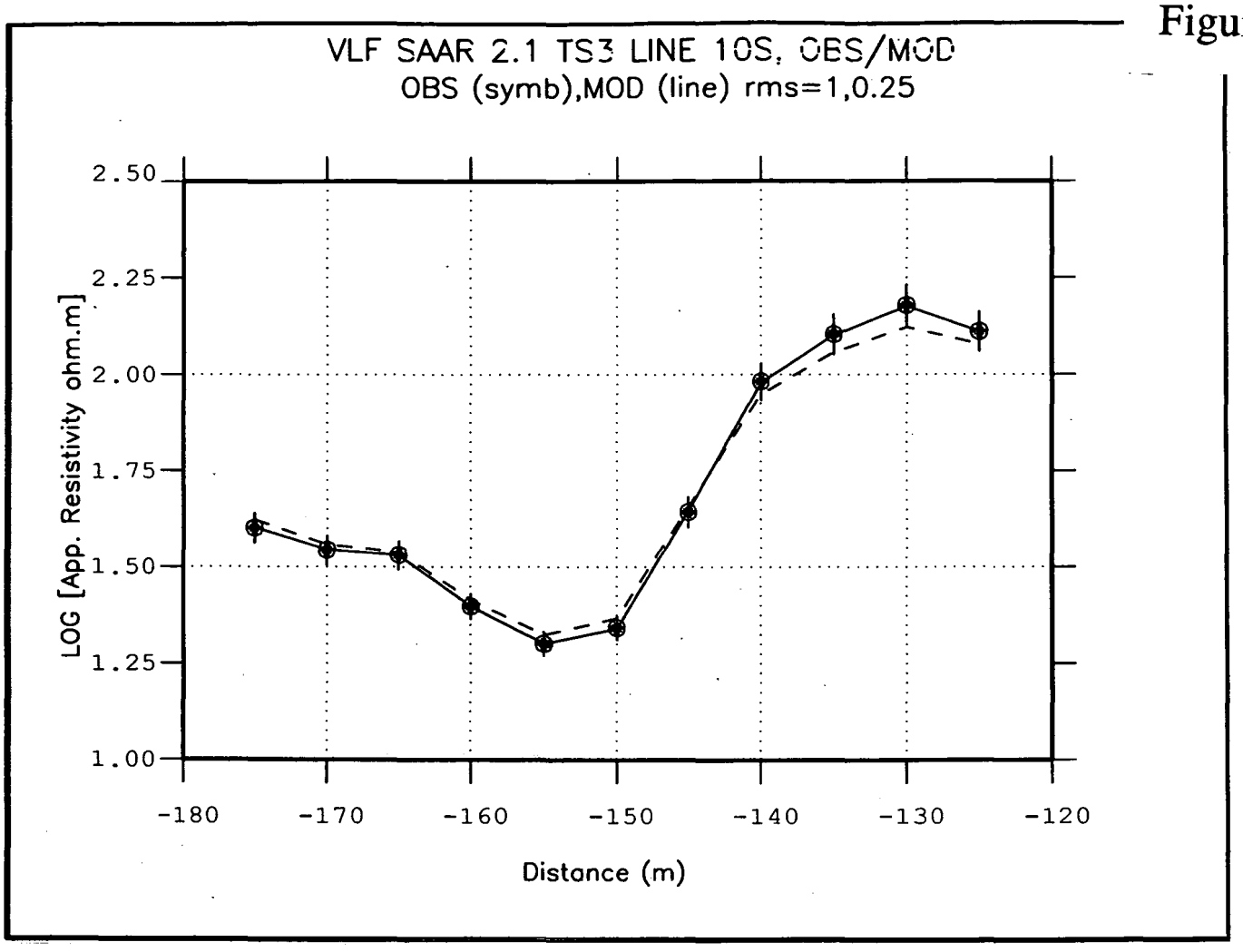
VLF SAAR 2.1 TS3 LINE 10S, OBS/MOD
OBS (symb),MOD (line) rms=1,0.25
LOG [App. Resistivity ohm.m]
2.50
2.25
2.00
1.75
1.50
1.25
1.00
-180
-170
-160
-150
-140
-130
-120
Distance (m)

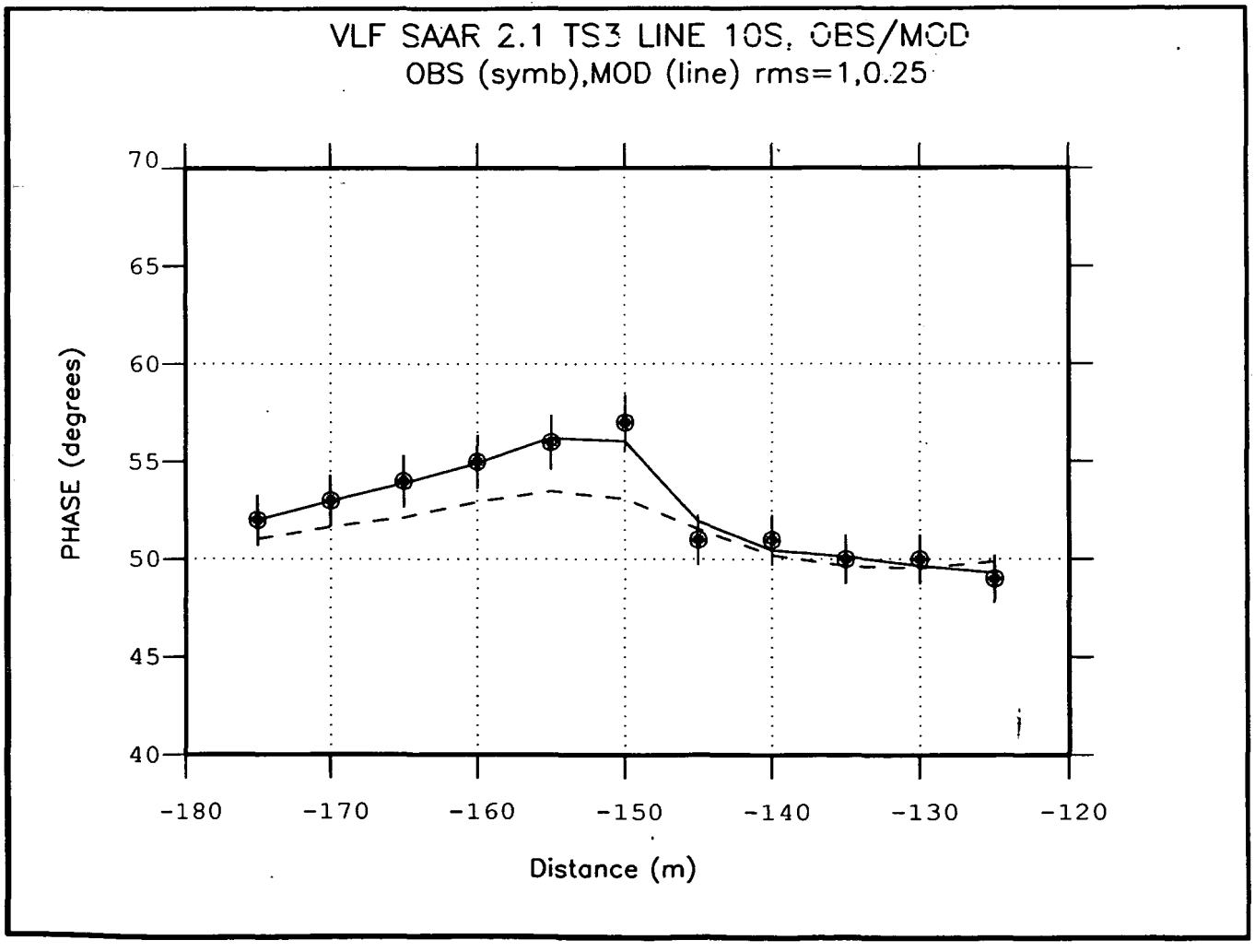
VLF SAAR 2.1 TS3 LINE 10S, OBS/MOD
OBS (symb),MOD (line) rms=1,0.25
PHASE (degrees)
70
65
60
55
50
45
40
-180
-170
-160
-150
-140
-130
-120
Distance (m)

Figure 14

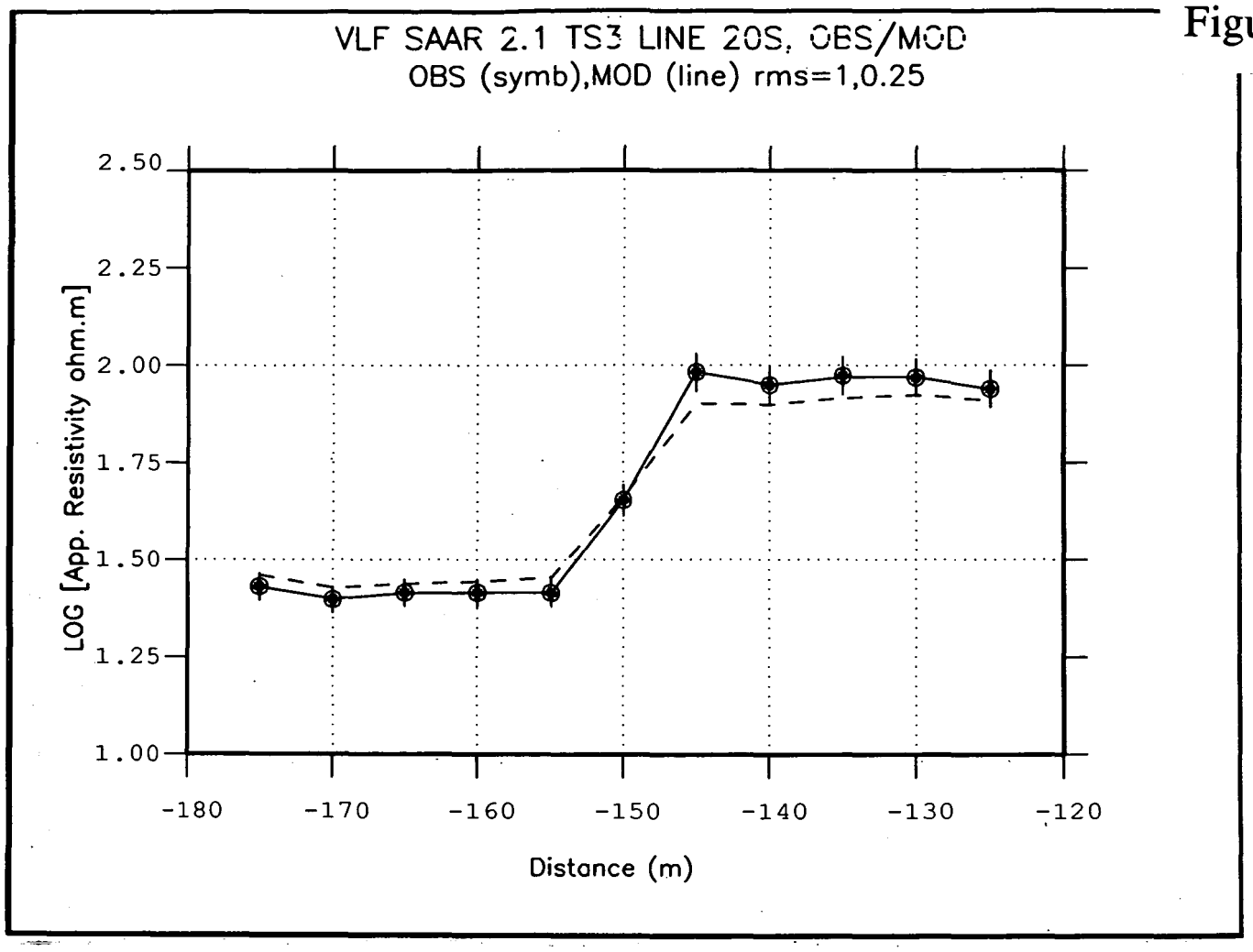
VLF SAAR 2.1 TS3 LINE 20S, OBS/MOD
OBS (symb),MOD (line) rms=1,0.25
LOG [App. Resistivity ohm.m]
2.50
2.25
2.00
1.75
1.50
1.25
1.00
-180
-170
-160
-150
-140
-130
-120
Distance (m)

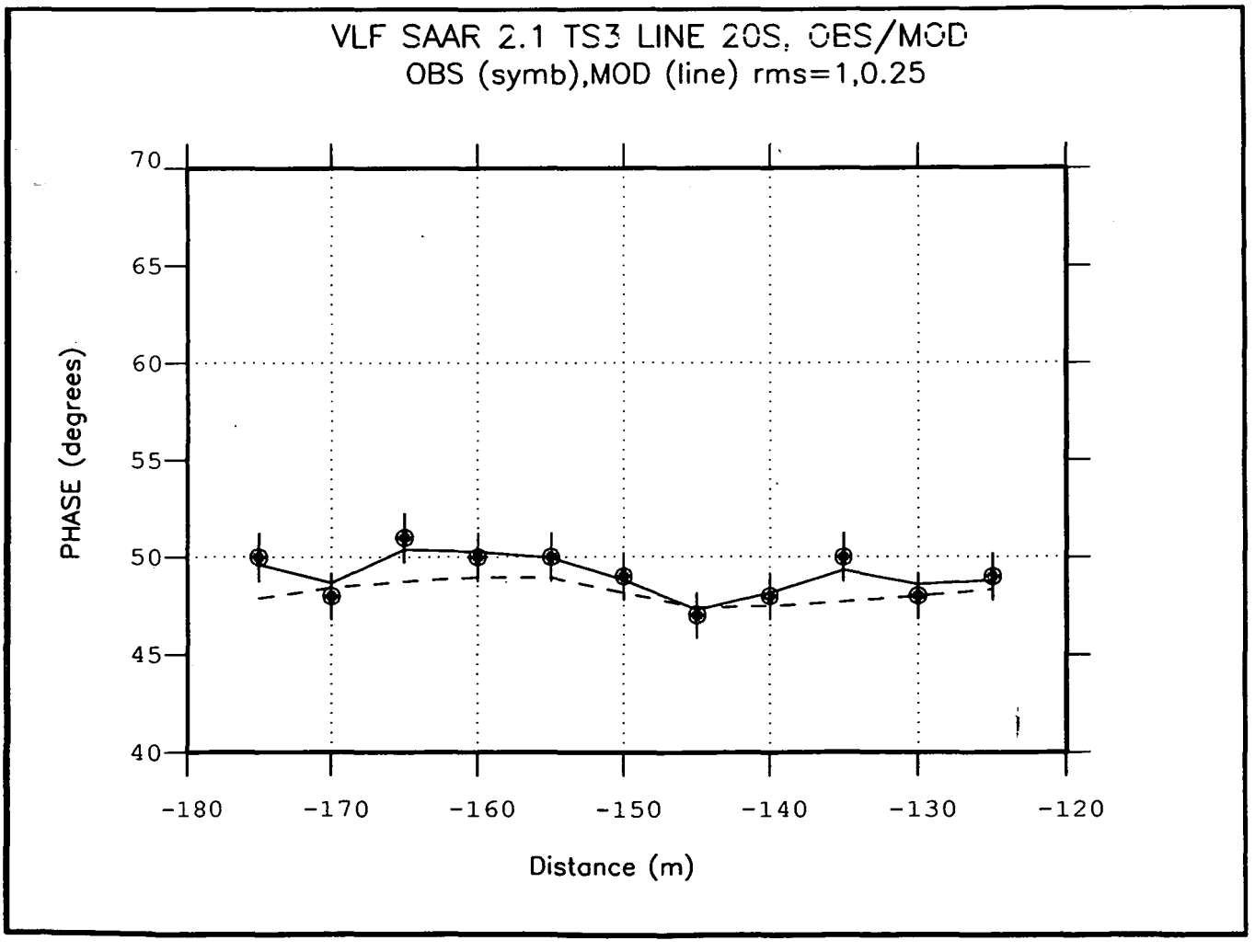
VLF SAAR 2.1 TS3 LINE 20S, OBS/MOD
OBS (symb),MOD (line) rms=1,0.25
PHASE (degrees)
70
65
60
55
50
45
40
-180
-170
-160
-150
-140
-130
-120
Distance (m)

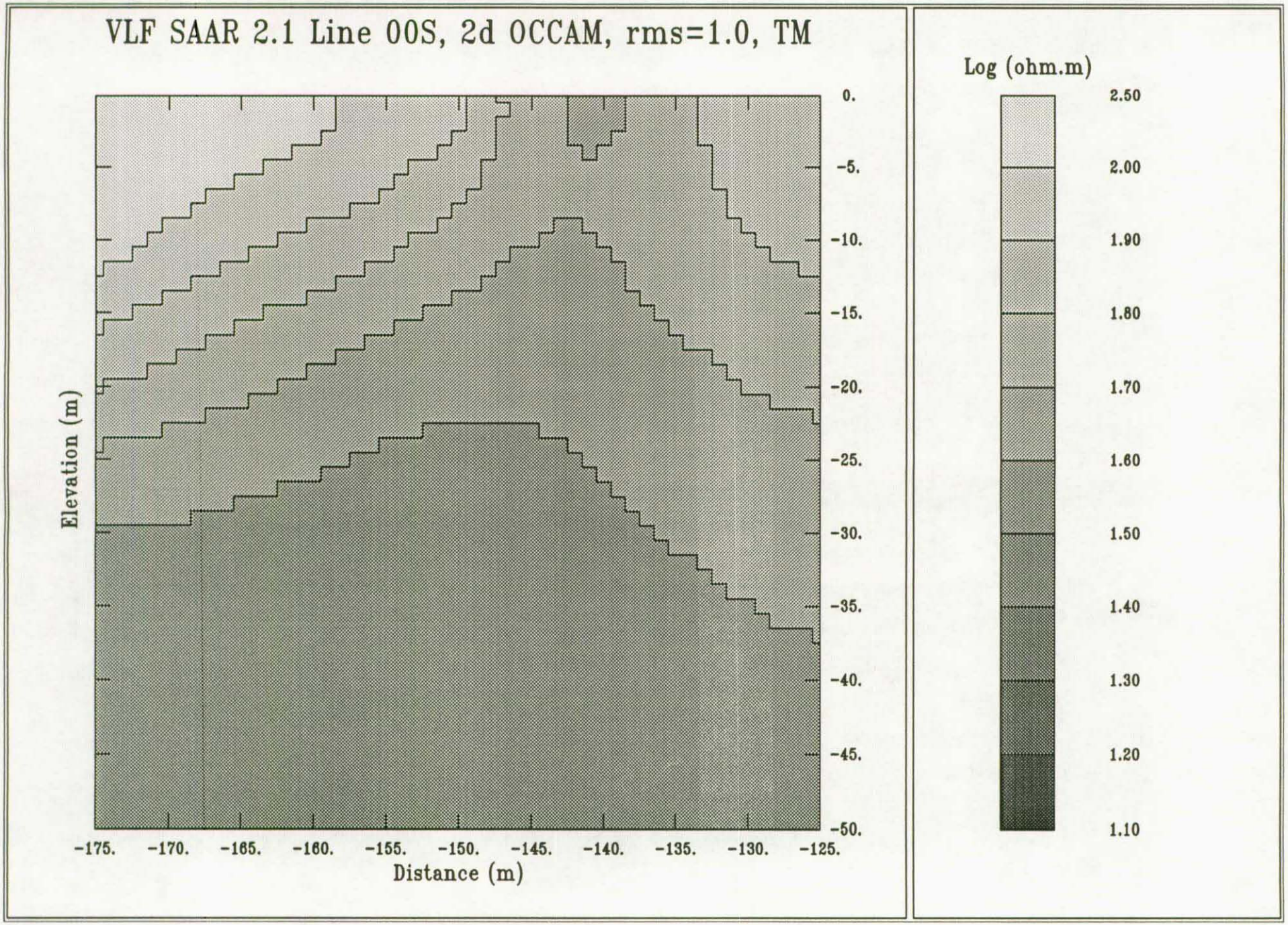
VLF SAAR 2.1 Line 00S, 2d OCCAM, rms=1.0, TM
Elevation (m)
0.
-5.
-10.
-15.
-20.
-25.
-30.
-35.
-40.
-45.
-50.
-175.
-170.
-165.
-160.
-155.
-150.
-145.
-140.
-135.
-130.
-125.
Distance (m)
Log (ohm.m)
2.50
2.00
1.90
1.80
1.70
1.60
1.50
1.40
1.30
1.20
1.10

Figure 15

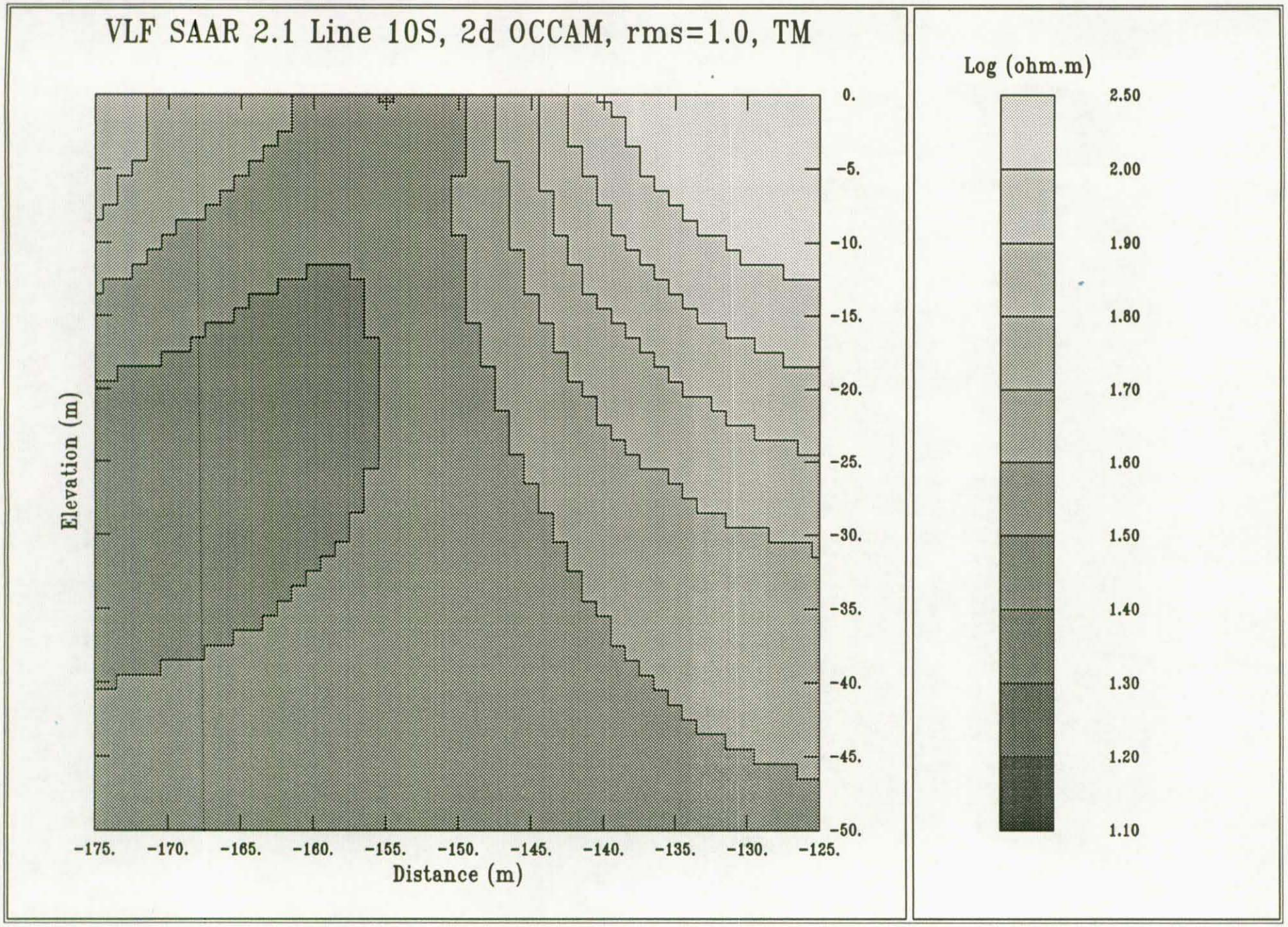
VLF SAAR 2.1 Line 10S, 2d OCCAM, rms=1.0, TM
Elevation (m)
0.
-5.
-10.
-15.
-20.
-25.
-30.
-35.
-40.
-45.
-50.
-175.
-170.
-165.
-160.
-155.
-150.
-145.
-140.
-135.
-130.
-125.
Distance (m)
Log (ohm.m)
2.50
2.00
1.90
1.80
1.70
1.60
1.50
1.40
1.30
1.20
1.10

Figure 16

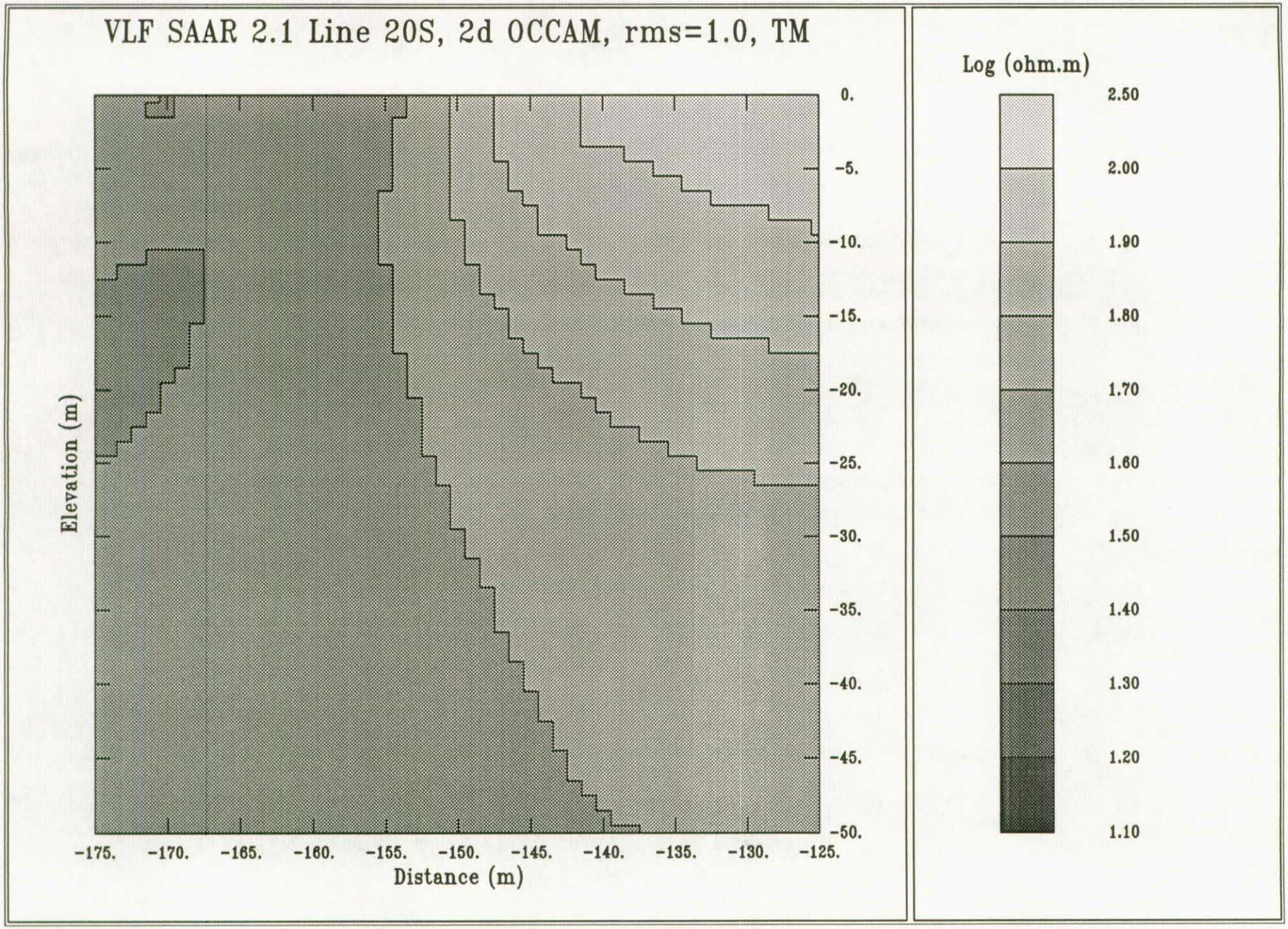
VLF SAAR 2.1 Line 20S, 2d OCCAM, rms=1.0, TM
Elevation (m)
0.
-5.
-10.
-15.
-20.
-25.
-30.
-35.
-40.
-45.
-50.
-175.
-170.
-165.
-160.
-155.
-150.
-145.
-140.
-135.
-130.
-125.
Distance (m)
Log (ohm.m)
2.50
2.00
1.90
1.80
1.70
1.60
1.50
1.40
1.30
1.20
1.10

Figure 17

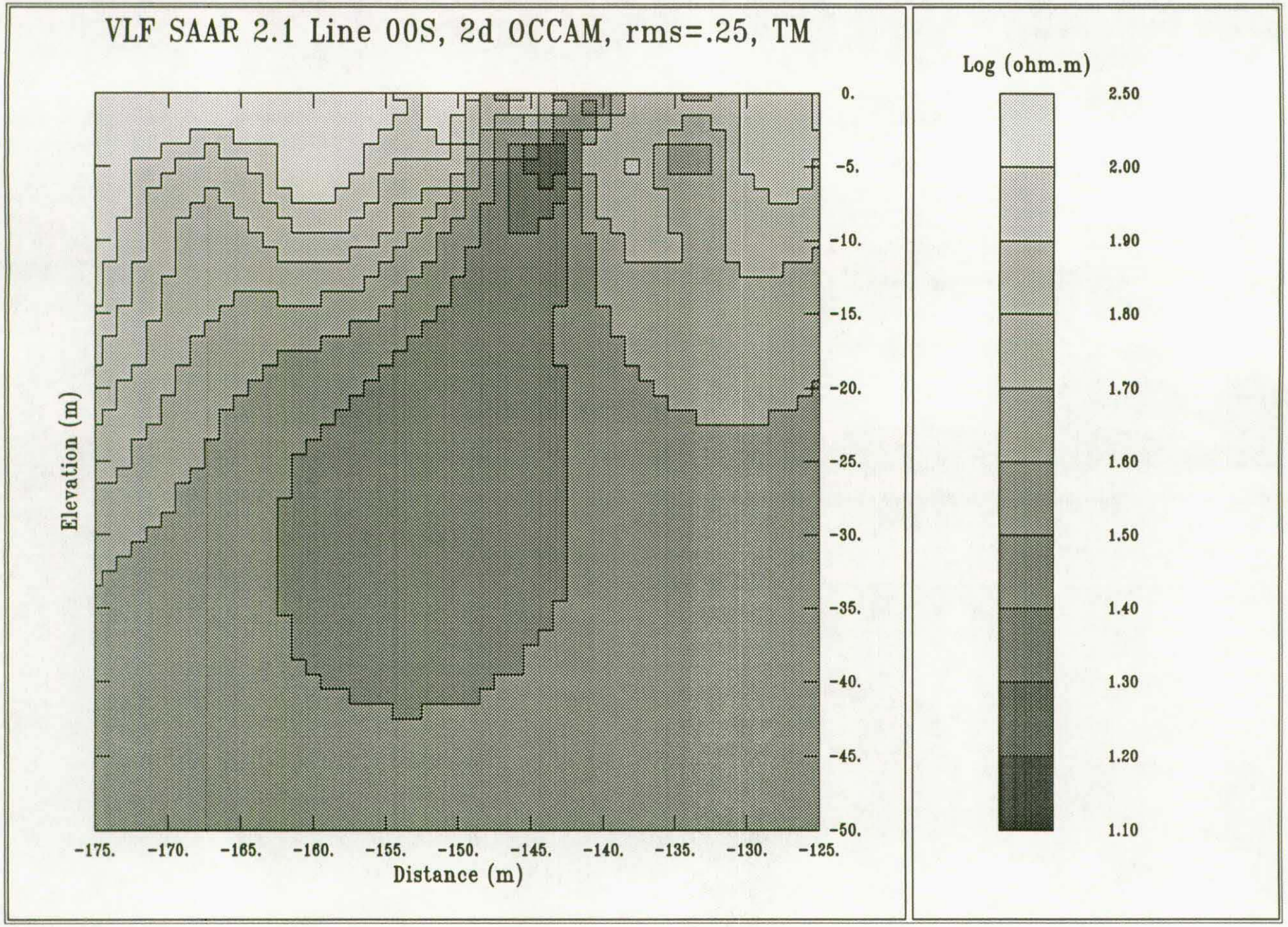
VLF SAAR 2.1 Line 00S, 2d OCCAM, rms=.25, TM
Elevation (m)
0.
-5.
-10.
-15.
-20.
-25.
-30.
-35.
-40.
-45.
-50.
-175.
-170.
-165.
-160.
-155.
-150.
-145.
-140.
-135.
-130.
-125.
Distance (m)
Log (ohm.m)
2.50
2.00
1.90
1.80
1.70
1.60
1.50
1.40
1.30
1.20
1.10

Figure 18

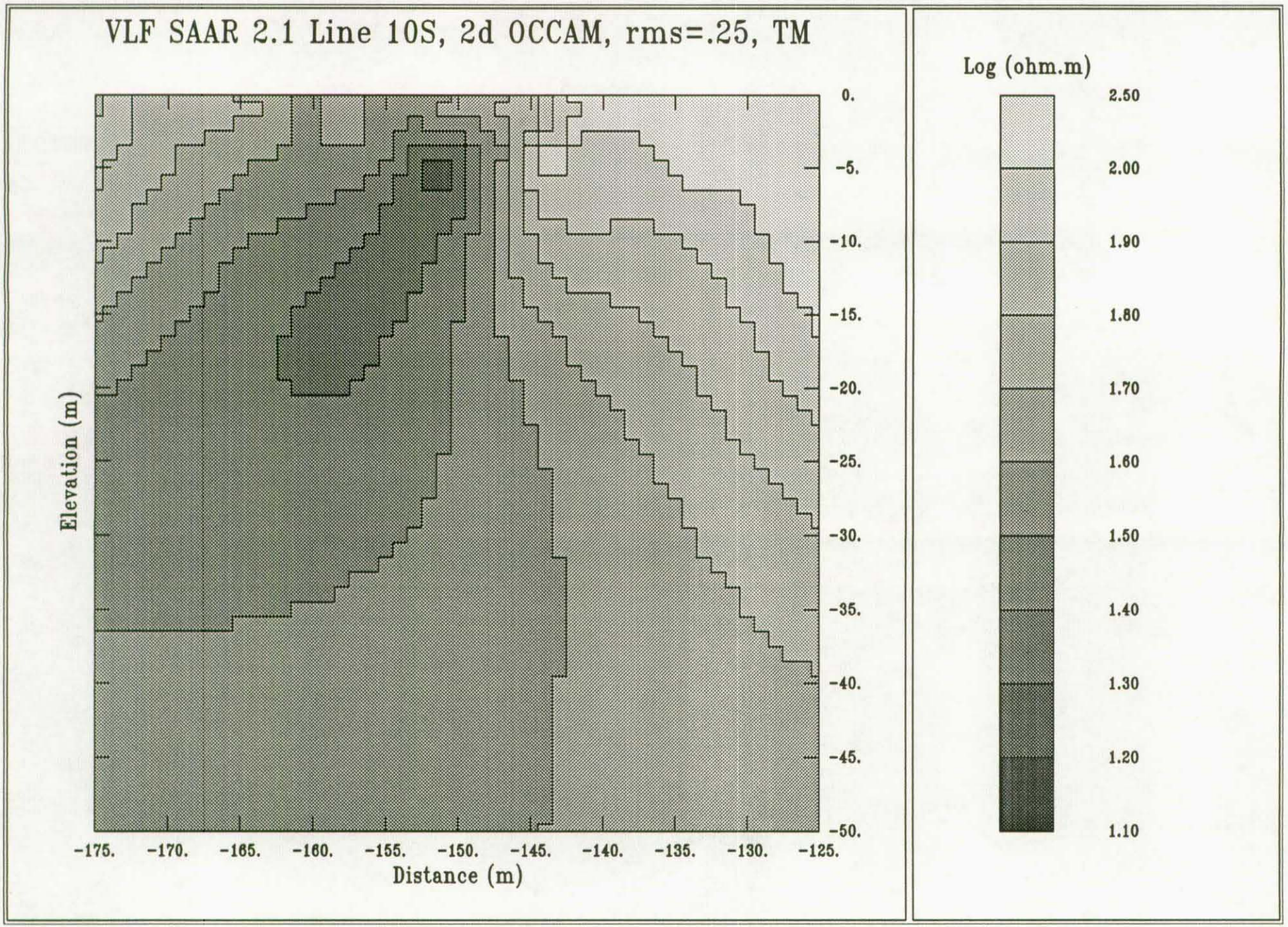
VLF SAAR 2.1 Line 10S, 2d OCCAM, rms=.25, TM
Elevation (m)
0.
-5.
-10.
-15.
-20.
-25.
-30.
-35.
-40.
-45.
-50.
-175.
-170.
-165.
-160.
-155.
-150.
-145.
-140.
-135.
-130.
-125.
Distance (m)
Log (ohm.m)
2.50
2.00
1.90
1.80
1.70
1.60
1.50
1.40
1.30
1.20
1.10

Figure 19

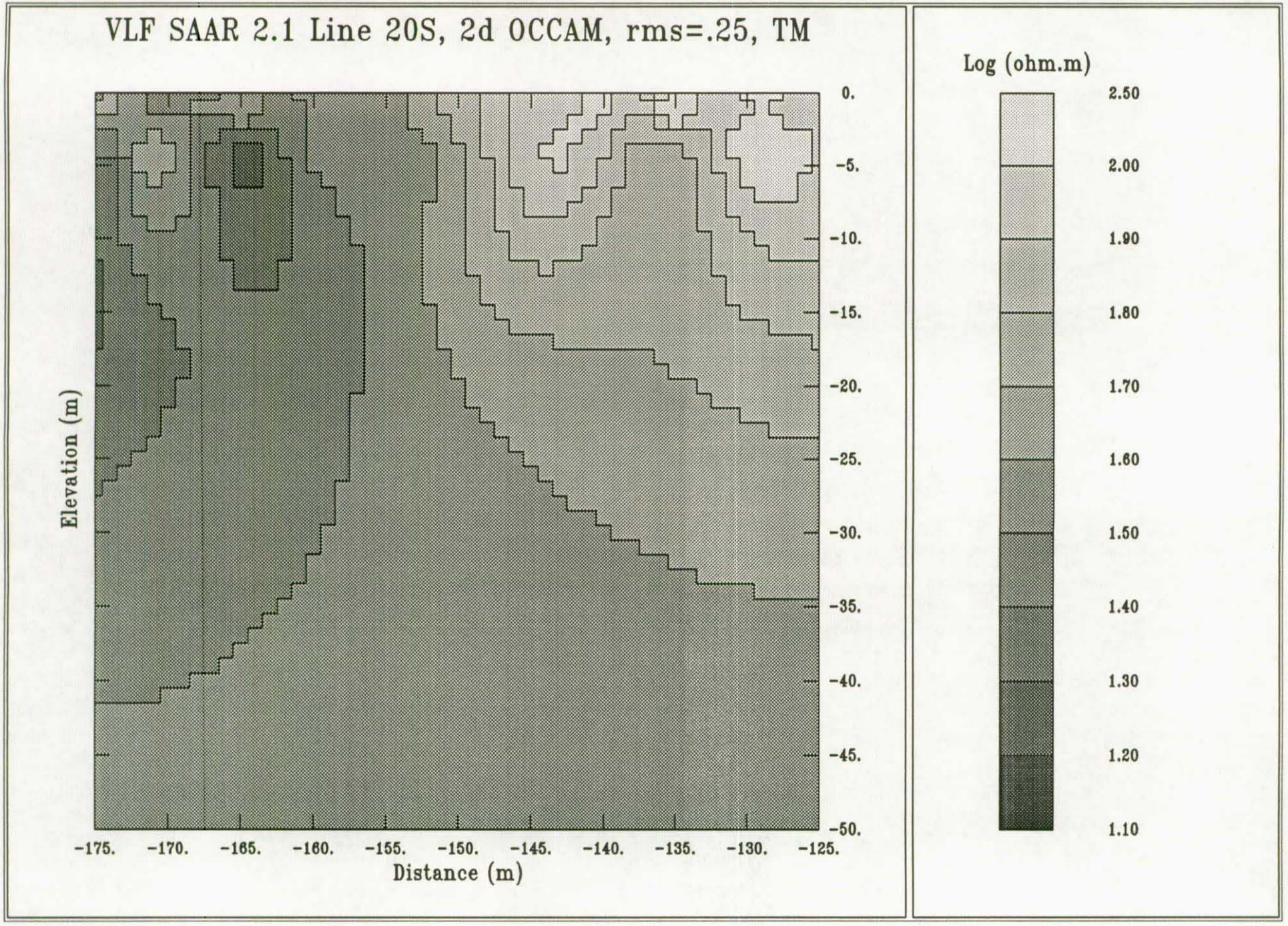
VLF SAAR 2.1 Line 20S, 2d OCCAM, rms=.25, TM
Elevation (m)
0.
-5.
-10.
-15.
-20.
-25.
-30.
-35.
-40.
-45.
-50.
-175.
-170.
-165.
-160.
-155.
-150.
-145.
-140.
-135.
-130.
-125.
Distance (m)
Log (ohm.m)
2.50
2.00
1.90
1.80
1.70
1.60
1.50
1.40
1.30
1.20
1.10

Figure 20